QUANTUM MEASUREMENT AND ITS APPLICATIONS IN QUANTUM OPTICAL SYSTEMS

A Dissertaion

by

LONGFEI FAN

Submitted to the Office of Graduate and Professional Studies of
Texas A&M University
in partial fulfillment of the requirements for the degree of

DOCTOR OF PHILOSOPHY

Chair of Committee,	M. Suhail Zubairy
Committee Members,	Aleksei Zheltikov
	Alexei Sokolov
	Philip Hemmer
Head of Department,	Grigory Rogachev

August 2018

Major Subject: Physics

ABSTRACT

Quantum measurement is the cornerstone of quantum computing and quantum information. It has many exciting applications. Various quantum optical systems are key to experimental physics because of their high precision and well controllability. In this dissertation, we focus on study of quantum measurement and its applications in quantum optical systems. We first study the fundamental trade-off relation between information gain and fidelity during successive weak QND measurement. Then we evaluate the effectiveness of quantum measurement reversal on quantum state protection under non-ideal detection efficiency. A linear optical setup is proposed for experimental verification of our result. Finally, we explore the performance of non-Gaussian two-mode entangled states for quantum illumination, which is an application of quantum state discrimination.

For successive weak QND measurements, we show that the information gain increases monotonically with respect to the number of measurements. Meanwhile the fidelity shows oscillatory decreasing behavior, which results from interference terms between photon numbers. We conclude that a greater information gain does not always imply a worse fidelity. For non-ideal quantum measurement reversal, we derive how quantum states evolve in quantum reversal under finite effective monitoring efficiency. Fidelity and concurrence are then calculated to evaluate the effectiveness of state protection using reversal. Generally the performance is weakened by finite monitoring efficiency. The negative effect of measurement reversal can dominate under certain conditions. A criterion that decides whether to apply state protection using measurement reversal is given. As for quantum illumination, we conclude that non-Gaussian operations can enhance the performance, i.e., achieve lower error probability by introducing both stronger entanglement and larger average photon numbers. However, if the signal strength is a concern, two-mode squeezed states (TMSS) performs better than other non-Gaussian states under the same output signal strength. When applying a coherent superposition of photon subtraction and photon addition to enhance quantum illumination, we show that optimal error probability is achieved by an asymmetrical operation.

DEDICATION

To my wife Xiaoshan Wang, my father Shanwei Fan, and my mother Xinai Sun for their love, encouragement, and support.

ACKNOWLEDGMENTS

I would like to express my sincere gratitude to my advisor, Dr. M. Suhail Zubairy, for his invaluable guidance and support throughout my PhD years. His immense knowledge, inspired ideas, and great patience are extraordinarily helpful for my study and research. I would like to thank Dr. Marlan O. Scully, who creates the exciting academic environment here at IQSE and offers me support. I would also like to thank Dr. Hyunchul Nha, whose enthusiasm and advice guide me at the beginning of my research. I am very thankful to my committee members, Dr. Alexei Sokolov, Dr. Aleksei Zheltikov, and Dr. Philip Hemmer, for their valuable comments on my research. I also appreciate Dr. Sokolov's guidance for the TAMU OSA student chapter when I volunteered as a board member there. I would also like to express my gratitude to all the faculty and staff of the Physics Department who have helped me.

Next I would like to thank my colleagues Dr. Wenchao Ge, Dr. Xiaodong Zeng, Dr. Zeyang Liao, and Dr. Yusuf Turek for their constructive discussions and fruitful collaborations. I am also very grateful to my friends, Dr. Yaodong Zhu, Dr. Yifeng Sun, Dr. Shuai Liu, Dr. Han Cai, Dr. Jabir Hakami, Minjie Lu, Gang Li, Yunsong Wu, Chao Fang, Zhongqu Long, Jieyu You, Saeed Asiri, and many more, for their help on my study and life.

Finally, I would like to express my gratitude to my parents, Shanwei Fan and Xinai Sun, and my sister, Xiaojie Fan, who are always unconditional supporters for my pursuits and dreams. Finally, I would greatly appreciate my wife, Xiaoshan Wang, who always encourages me with her great enthusiasm, stays with me to overcome obstacles, and brings me endless happiness.

CONTRIBUTORS AND FUNDING SOURCES

Contributors

This work was supported by a dissertation committee consisting of Professors M. Suhail Zubairy (advisor), Aleksei Zheltikov, and Alexei Sokolov of the Department of Physics and Astronomy and Professor Philip Hemmer of the Department of Electrical and Computer of Engineering.

The ininitial research ideas in Chapter 2, Chapter 3, and Chapter 4 were proposed by Professor M. Suhail Zubairy of the Department of Physics. The second definition of fidelity in Chapter 2 was proposed by Professor Hyunchul Nha of the Department of Physics of Texas A&M University at Qatar. Some analysis of coherent states in Chapter 2 was completed by Dr. Wenchao Ge of Department of Physics.

All other work conducted for the dissertation was completed by the student independently.

Funding Sources

The research in Chapter 2 was supported by a NPRP Grant (No. 5-102-1-026) from the Qatar National Research Fund. The research in Chapter 3 and Chapter 4 was supported by a NPRP Grant (No. 8-751-1-157) from the Qatar National Research Fund. Graduate study was supported by a fellowship from the Heep Foundation.

NOMENCLATURE

QND	Quantum Non-Demolition
$I(X;Y)$	Mutual Information between Two Sets of Random Variables
$F(\rho_1, \rho_2)$	Fidelity between Two Density Matrices
AD	Amplitude Damping
$C(\rho)$	Concurrence of A Density Matrix
PBS	Polarization Beam Splitter
BS	Beam Splitter
HWP	Half-Wave Plate
TMSS	Two-Mode Squeezed State
PS	Photon Subtraction
PA	Photon Addition
PSA	Photon Subtraction following Addition
PAS	Photon Addition following Subtraction
PCS	Coherent Superposition of Photon Subtraction and Addition
QCB	Quantum Chernoff Bound

TABLE OF CONTENTS

Page

LIST OF FIGURES

FIGURE Page

1. INTRODUCTION

Quantum measurement lies in the core of fundamental quantum physics. It has many applications in quantum information, quantum computation, quantum metrology, and quantum control [1, 2, 3, 4]. Quantum optical systems are important platforms for physical implementations of these applications [5, 6].

One fundamental and practical problem in quantum information processing is the trade-off relation between information gain and state disturbance during quantum measurement. In order to obtain information of a quantum system, we must make measurements on it, which will inevitably bring disturbance to the system at the same time. In projective measurement, which is also named Von Neumann measurement [7], the system collapses to one of the eigenstates corresponding to the observable to be measured. In generalized quantum measurement, the measurement strength can be controlled such that a weak measurement can be made. In weak measurement, states will collapse partially rather than completely to eigenstates. As a sacrifice, little information is extracted during week measurement.

The trade-off relation between information and disturbance has been studied from various aspects [8, 9, 10, 11, 12, 13, 14, 15, 16, 17]. The information gain can quantified by estimation fidelity [9, 11, 13, 17], by mutual information [12], and by change of entropy [8, 15, 16]. The output fidelity with respect to an initial state can be used as a measure of disturbance. The reversibility has also been studied [18, 19, 20, 21, 22, 23, 24, 25, 26] as a measure of disturbance. A quantitative balance between information gain and disturbance has been studied under different circumstances [8, 9, 11, 12, 13, 14, 15, 16, 17].

Quantum coherence and quantum entanglement are key quantum resources for quantum information processing [1]. However, they are vulnerable to quantum decoherence. Various protections methods have been proposed to protect them against decoherence to realize practical quantum technologies, including quantum error correction [27, 28, 29, 30, 31], surface codes [32, 33], topological quantum computation [34, 35, 36, 37], decoherence-free subspace [38, 39, 40], and

dynamical decoupling [41, 42, 43, 44, 45]. Recently, suppressing amplitude-damping decoherence using partial measurement and quantum reversal [46, 47, 48, 49] has been proposed. Reversing quantum states has been studied on solid-state qubits [50, 51], cavity field states [52], polarized photonic qubits [53], and bi-particle entanglement states [54] in the latest decade. The underlying fact of quantum reversal is that quantum states may collapses partially after a weak measurement. If the states are monitored, uncollapsed outcomes of measurement can be collected exclusively and reversed by proper operations. Quantum reversal can also be realized with quantum gates [55, 56, 57, 58].

Later, a three-stage protocol [59] is proposed to protect quantum states from amplitude damping. Firstly it applies a monitored partial measurement to bring a qubit closer to its ground state in a coherent but non-unitary way [60, 59]. Thus the qubit is less vulnerable in the later amplitude-damping process. After that uncollapsed states will be selected and recovered by the usual quantum reversal method. Following the linear optical setup proposed by Q. Sun, $et\ al.$ [54], the protocol has been demonstrated experimentally to protect photonic qubits [61] and their entanglement [62, 63, 64] from artificially generated damping. Meanwhile it has been realized to protect practical superconducting qubits [65] against energy relaxation. The protocol has also been applied to manipulate and enhance two-qubit entanglement [66, 67], and some other applications [68, 69, 70, 71]. Similar protocols have been proposed to protect quantum states against other decoherence processes like generalized amplitude damping [72] and depolarization[73].

To monitor the state of a target system which needs protection is the crucial key of the three-stage protection. The monitoring efficiency must be 100% to collect all the uncollapsed states and discard all the collapsed ones. A strong projective measurement on the target system will obviously destroy their states. Thus an auxiliary system which can interact with the target system in a controllable manner is necessary. In recent studies, fields outside a leaky cavity [52] and a qubit whose state can be swapped with that of the target qubit [65] are utilized as auxiliary systems. The former uses an ideal photon detector to monitor the fields. The latter requires a readout of the states of superconducting qubits, whose fidelity varies from 88% to 98% in up-to-

date technology [65, 74]. Detection-free method with perfect 100% efficiency is implemented in linear optical systems [53, 54, 61, 62, 63, 64]. However, it may not be applied to other physical schemes straightforwardly.

Non-Gaussian quantum resources play importance roles in quantum information [75]. Photon subtraction and photon addition can generate non-Gaussian states with enhanced entanglement and quantum correlation [76, 77, 78]. Entanglement is regarded as the key resource assisting quantum illumination [79, 80, 81]. It has been shown that a photon-subtracted TMSS can achieve lower error probability [82], where the performance is compared under the same squeezing strength of detecting states. Coherent superposition of photon subtraction and addition can enhance entanglement more than mere subtraction and addition, particularly in small squeezing regime [83, 84], in which quantum illumination also has the most advantages [79, 81, 80]. Thus we could expect coherent superposition of photon subtraction and addition can enhance quantum illumination more than other non-Gaussian operations.

The above paragraph shows that our physical intuition on how to choose better detecting states is obtained from looking into entanglement of states. It has to be mention that besides entanglement, mutual information and quantum discord [85, 86] have also been shown to be the source assisting quantum illumination [87, 88, 89]. Quantum discord explains the resilience of quantum illumination in entanglement-breaking channel. Here we only focus on comparison of entanglement, which will be shown in our results to give useful hints on choosing better detecting states for quantum illumination.

Non-Gaussian resources play importance roles in quantum information [75]. Photon subtraction and photon addition can generate non-Gaussian states which have enhanced entanglement and quantum correlation [76, 77, 78]. As entanglement is regarded as the key resource assisting quantum illumination, it has been showed that a photon-subtracted TMSS can achieve lower error probability [82], where the performance is compared under the same squeezing strength of detecting states. A coherent superposition of photon subtraction and addition can enhance entanglement more than mere subtraction and addition, particularly in small squeezing regime [83, 84], where

quantum illumination also performs most effectively [79, 81, 80]. Thus we can expect a coherent operation can enhance quantum illumination more than other non-Gaussian operations.

This dissertation is organized as follows. In Chapter 2, we show the trade-off relation between information gain and fidelity with a weak quantum non-demolition model. Photonic qubit states and coherent states are used as quantum system to be measured. In Chapter 3, we study the non-ideal quantum measurement reversal and its applications in quantum state and entanglement protection. We verify our theory and results in a linear optical system. In Chapter 4, we compare the performance of various non-Gaussian states for quantum illumination. Finally, we give our summary and conclusion in Chapter 5.

2. TRADE-OFF BETWEEN INFORMATION GAIN AND FIDELITY UNDER WEAK MEASUREMENTS *

In this chapter, we study the tradeoff between the information gain and the output fidelity in a QND measurement of photon numbers [90]. In a QND measurement based on a cavity-QED setup, the measurement outcomes are binary, i.e., distinction between two atomic states, and an initial cavity state may collapse to a Fock state only after many successive measurements [91]. In this respect, a single QND measurement in our study is a weak measurement and the measurement strength can be adjusted by changing the experimental parameters.

We consider that the cavity is initially prepared in an unknown pure state $|\psi\rangle$ with a given probability density $p(\psi)$. The information gain may be quantified as the decrease of the Shannon entropy of the cavity state under the QND measurement, i.e. mutual information. We also introduce another measure of information gain, which is closely related to the concept of classical fidelity. We then investigate the tradeoff relation between the information gain on the unknown state and the disturbance of the state by varying the coupling strength or the number of successive measurements. Our results show that more information gain does not always lead to worse fidelity.

This chapter is organized as follows. In Sec. 2.1, we present our scheme for a QND measurement of photon numbers and give general expressions for information gain and output fidelity after N sequential measurements. We illustrate the tradeoff relations with two specific classes of cavity states in Sec. 2.2.

2.1 The scheme and theory analysis

2.1.1 QND measurements of photon numbers

We first introduce the scheme used for a QND measurement of photon numbers based on a cavity-QED setup [90]. This scheme makes it possible to gain information on the distribution of

*Reprinted with permission from "Trade-off between information gain and fidelity under weak measurements" by Longfei Fan, Wenchao Ge, Hyunchul Nha, and M. Suhail Zubairy, Phys. Rev. A 92, 022114 (2015), Copyright [2015] by the American Physical Society.

photon numbers of a cavity field without absorbing the photons (Fig. 2.1). Suppose that the state of the system prepared in a high-Q cavity (C in Fig. 2.1) is a pure state $|\psi\rangle$ with its probability distribution $p(\psi)$. A three level atom (measuring device), with the level diagram in Fig. 2.2, is initially prepared in the $|e\rangle$ state. The initial state of the system and the device is given by

$$\rho_{sd} = \rho_s \otimes \rho_d = \sum_{\psi} p(\psi)|\psi\rangle\langle\psi| \otimes |e\rangle\langle e|, \tag{2.1}$$

where $p(\psi)$ is the probability of each state $|\psi\rangle$ to be prepared inside the cavity. In the remainder of this article, we use the term "information" to refer how well we know about which state $|\psi\rangle$ is prepared in the cavity out of the ensemble $\sum_{\psi} p(\psi)|\psi\rangle\langle\psi|$. That is to say, we measure a single system to guess which $|\psi\rangle$ is the most likely input state given a measurement output.

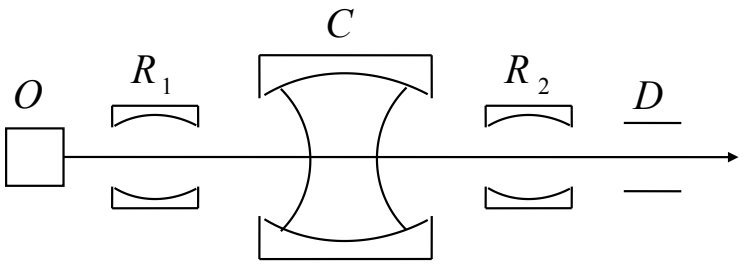

Figure 2.1: QND measurement scheme. The field is initially prepared in a high-Q cavity C interacting with traveling atoms. The atoms are prepared and velocity-selected in the box O, then pass through the three cavities. In each cavity of R_1 and R_2, the atom undergoes a $\pi/2$ transformation. Finally, the ionized counter D detects whether each atom is in state $|e\rangle$ or state $|f\rangle$.

Inside the cavity, the atom interacts with the field, which is described by

$$H = \frac{1}{2}\hbar\omega_{ie}\sigma_z + \hbar\omega a^\dagger a + \hbar g\left(a\sigma_+ + a^\dagger\sigma_-\right), \tag{2.2}$$

where a ($a^\dagger$) is the cavity photon annihilation (creation) operator, $\sigma_- = |e\rangle\langle i|$, $\sigma_+ = |i\rangle\langle e|$, $\sigma_z = \sigma_+\sigma_- - \sigma_-\sigma_+$, and g the atom-cavity coupling strength. The atomic level $|f\rangle$ is not involved in the interaction. When the cavity-field frequency ω is detuned by an amount Δ from the atomic

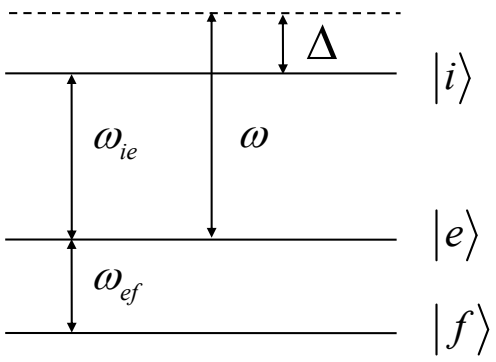

Figure 2.2: Atom levels used for detecting states of the cavity field.

transition frequency ω_{ie}, the effective interaction becomes a dispersive coupling described by[5]

$$V = \frac{\hbar g^2}{\Delta} a^\dagger a |e\rangle\langle e|. \tag{2.3}$$

After an interaction time τ, the evolution operator is given by

$$U_I = \exp(-iV\tau/\hbar) = \exp\big(-i\varphi a^\dagger a |e\rangle\langle e|\big), \tag{2.4}$$

where $\varphi \equiv g^2\tau/\Delta$ is the phase shift caused by one photon, which characterizes the coupling strength between the atom and the field. This interaction leads to a phase shift on $|e\rangle$ state, which is proportional to the photon numbers.

The phase shift can be detected with Ramsey interferometric method [92], in which the atom undergoes $U_{\pi/2}$ transformations before and after the cavity C, where

$$U_{\pi/2} = \frac{1}{\sqrt{2}}(|e\rangle\langle e| + |f\rangle\langle f| + i|e\rangle\langle f| + i|f\rangle\langle e|) \tag{2.5}$$

Finally, we use an ionized detector to make a projective measurement on the atom represented by the operators

$$P_m = |m\rangle\langle m|, \quad m = e, f. \tag{2.6}$$

Given the outcome m, the operation made is described by

$$U_m = P_m U_{\pi/2} U_I U_{\pi/2}. \tag{2.7}$$

After such an operation, the density operator evolves to

$$\rho_{sd,m} = U_m \rho_{sd} U_m^\dagger. \tag{2.8}$$

We are interested in the state of the system only. Tracing over the device and normalizing, we obtain the density operator of the system

$$\rho_{s,m} = \frac{\mathrm{Tr}_d(U_m \rho_{sd} U_m^\dagger)}{\mathrm{Tr}(U_m \rho_{sd} U_m^\dagger)} = \frac{M_m \rho_s M_m^\dagger}{\mathrm{Tr}_s(M_m \rho_s M_m^\dagger)}, \tag{2.9}$$

where Tr_s (Tr_d) denotes tracing over the system (device) and Tr represents tracing over both the system and the device. The measurement operators M_m are derived according to Kraus representation theory as

$$\begin{aligned} M_e &= \langle e|U_e|e\rangle = \left[\exp\left(-i\varphi a^\dagger a\right) - 1\right]/2, \\ M_f &= \langle f|U_f|e\rangle = \left[\exp\left(-i\varphi a^\dagger a\right) + 1\right]/2. \end{aligned} \tag{2.10}$$

In the Fock-state basis, they can be expressed by

$$\begin{aligned} M_e &= \sum_{n=0}^{n_{\max}} \frac{\exp(-in\varphi) - 1}{2} |n\rangle\langle n|, \\ M_f &= \sum_{n=0}^{n_{\max}} \frac{\exp(-in\varphi) + 1}{2} |n\rangle\langle n|. \end{aligned} \tag{2.11}$$

It can be readily checked that the relation $\sum_{m=e,f} M_m^\dagger M_m = I$ is satisfied, implying that our QND measurement is a general quantum measurement with two outcomes.

The probability of obtaining outcome m is given by

$$p(m) = \mathrm{Tr}_s(M_m \rho_s M_m^\dagger) = \sum_\psi p(\psi) p(m|\psi), \tag{2.12}$$

where the conditional probability of output m given input $|\psi\rangle$ is

$$p(m|\psi) \equiv \mathrm{Tr}_s(M_m |\psi\rangle\langle\psi| M_m^\dagger). \tag{2.13}$$

2.1.2 Measurements with N successive atoms

Suppose now that we make N successive QND measurements. Given that N_e atoms are found in $|e\rangle$ state and $N_f = N - N_e$ atoms in $|f\rangle$ state, the state of the cavity field becomes (we omit the symbol s on the density operator of the system in the remaining part.)

$$\rho_{N_e} = \frac{M_{N_e} \rho M_{N_e}^\dagger}{\mathrm{Tr}_s(M_{N_e} \rho M_{N_e}^\dagger)}, \tag{2.14}$$

where the measurement operator reads

$$M_{N_e} = M_e^{N_e} M_f^{N-N_e}. \tag{2.15}$$

We here assume that the coupling strength φ is the same for each measurement for simplicity. We note that M_e and M_f commute with each other, so the order of the operators does not affect the results. From an information-theoretic perspective, it means that no extra information can be obtained by keeping record of the sequence of measurement outputs, therefore one only needs to count N_e, the number of atoms in $|e\rangle$. There are $C_N^{N_e} \equiv \frac{N!}{N_e!(N-N_e)!}$ cases to obtain N_e counts and it follows

$$\sum_{N_e=0}^{N} C_N^{N_e} M_{N_e}^\dagger M_{N_e} = I, \tag{2.16}$$

meaning that counting the number N_e also represents a general quantum measurement with $N+1$ different outcomes.

The probability to get output N_e is

$$p(N_e) \equiv C_N^{N_e} \mathrm{Tr}_s(M_{N_e} \rho M_{N_e}^\dagger) = \sum_\psi p(\psi) p(N_e|\psi), \tag{2.17}$$

where the conditional probability of N_e given ψ is

$$p(N_e|\psi) \equiv C_N^{N_e} \mathrm{Tr}_s(M_{N_e} |\psi\rangle\langle\psi| M_{N_e}^\dagger) \tag{2.18}$$

In Fock-state basis, a random state can be expressed as $|\psi^k\rangle = \sum_{n=0}^{n_{\max}} b_n^k |n\rangle$. The above probability is then expressed as

$$P(N_e|\psi^k) = C_N^{N_e} \sum_n |b_n^k|^2 c_n^{2N_e} d_n^{2(N-N_e)}, \tag{2.19}$$

where $c_n = \sin\left(\frac{n\varphi}{2}\right)$, and $d_n = \cos\left(\frac{n\varphi}{2}\right)$.

2.1.3 Information gain via the mutual information

Next we introduce a measure of information gain—mutual information. Suppose that we have a black box (an operation) with an input port and an output port. The input random variable x is chosen from a set $\{x \in X\}$ with a prior probability $p(x)$. The output is chosen from the set $\{y \in Y\}$. The black box is modeled by transfer probability $p(y|x)$. Shannon entropy [93] for the set $\{x \in X\}$ is defined as

$$H(X) = -\sum_x p(x) \log_2 p(x), \tag{2.20}$$

which quantifies the lack of information on events X. Given an output y, we obtain a conditional probability $p(x|y) = p(y|x)p(x)/p(y)$, which leads to the conditional entropy

$$H(X|Y) = -\sum_y p(y) \sum_x p(x|y) \log_2 p(x|y). \tag{2.21}$$

The conditional probability measures how much information for X is still missing after we have known Y. Thus the difference between the original entropy $H(X)$ and the conditional entropy $H(X|Y)$ may be regarded as the information gain. This so-called mutual information [93, 94, 95]

is defined by

$$\begin{aligned} I(X;Y) &= H(X) - H(X|Y) \\ &= \sum_x \sum_y p(x,y) \log_2 \frac{p(x,y)}{p(x)p(y)}, \end{aligned} \tag{2.22}$$

In our case, the input random variable is chosen from all possible cavity states $\{|\psi^k\rangle\}$ with a prior probability $p(\psi^k)$. The output random variable is the count N_e under N measurements. Eq (2.22) is then written by replacing $x \to \psi^k$, and $y \to N_e$, which gives the mutual information as

$$I_M = \sum_{N_e=0}^{N} \sum_k p(N_e|\psi^k) p(\psi^k) \log_2 \frac{p(N_e|\psi^k)}{p(N_e)}. \tag{2.23}$$

Plugging Eqs. (2.17) and (2.19) into Eq. (2.23), we can calculate the information gain.

2.1.4 Information gain via the probability overlap

Instead of the mutual information I_M in Eq. (2.23) adopting the entropies of relevant probability distributions, we may characterize the information gain in another form, which can have a conceptual connection to fidelity. Given two probability distributions $p_1(x)$ and $p_2(x)$, their distinction can be measured by $1 - F_c^2$, where F_c is the classical fidelity quantifying their overlap as

$$F_c(p_1, p_2) = \sum_x \sqrt{p_1(x) p_2(x)}. \tag{2.24}$$

If the probability distribution $p_1 = p(\psi^k|N_e)$ conditioned on the measurement outcome N_e becomes more distinguishable from a completely random distribution $p_2(x) = 1/N$ than the initial distribution $p_1 = p(\psi^k)$, it may represent information gain through our QND measurement. Thus, using

$$I_F[p(x)] \equiv 1 - \left(\sum_x \sqrt{p(x)/N} \right)^2. \tag{2.25}$$

we may define another measure of information gain as

$$I_F = \sum_k p(\psi^k) \sum_{N_e} p(N_e) I_F[p(\psi^k|N_e)] - I_F[p(\psi^k)], \tag{2.26}$$

where the subscript F refers to the conceptual connection to fidelity. In this paper, we use two quantifiers I_M in Eq. (2.23) and I_F in Eq. (2.26) to measure information gain under QND measurements.

2.1.5 Fidelity

On the other hand, we use the output fidelity as a measure of disturbance due to quantum measurement. The fidelity [9] of the output state is defined to be the average overlap between the input state $|\psi^k\rangle$ and the output state $M_{N_e}|\psi^k\rangle$, given by

$$F = \sum_k p(\psi^k) \sum_{N_e=0}^{N} C_N^{N_e} |\langle\psi^k|M_{N_e}|\psi^k\rangle|^2. \tag{2.27}$$

By substituting Eq. (2.15), we obtain the expression of fidelity in Fock state basis as

$$F = \sum_k p(\psi^k) \sum_{N_e=0}^{N} C_N^{N_e} \left| \sum_n^{n_{\max}} |b_n^k|^2 e^{-\frac{iNn\varphi}{2}} c_n^{N_e} d_n^{N-N_e} \right|^2. \tag{2.28}$$

2.2 Tradeoff relations

Having obtained the general expressions for the information gain and the output fidelity, we now consider some classes of states to investigate the tradeoff relation under varying experimental conditions.

2.2.1 Photonic qubit states

We here consider an initial state of the cavity field as an unknown superposition of the vacuum and the single-photon states chosen from the following mixture with probability density $p(\theta, \phi)$,

$$\rho = \sum_{\theta,\phi} p(\theta, \phi) |\psi_{\theta,\phi}\rangle\langle\psi_{\theta,\phi}|, \tag{2.29}$$

where the photonic qubit state

$$|\psi_{\theta,\phi}\rangle = \cos(\theta/2)|0\rangle + \sin(\theta/2)e^{i\phi}|1\rangle. \tag{2.30}$$

We assume that this unknown state is uniformly distributed in the Bloch sphere so that the probability density is

$$p(\theta, \phi) = 1/4\pi. \tag{2.31}$$

Since it is a continuous distribution, we convert the summation to an integral as

$$\sum_{\theta,\phi} p(\theta, \phi) \to \frac{1}{4\pi} \int_0^{\pi} \mathrm{d}\theta \sin\theta \int_0^{2\pi} \mathrm{d}\phi, \tag{2.32}$$

and study the tradeoff under different coupling strengthes and the number of measurements. It is straightforward to obtain

$$\begin{aligned} F(N, \varphi) &= \frac{2}{3} + \frac{1}{3}\cos(N\varphi/2)\cos^N(\varphi/2), \\ I_M(N, \varphi) &= 1 - \frac{1}{2\ln 2} - \frac{1}{2}\cos^{4N}(\varphi/2)\log_2\cos^{2N}(\varphi/2) \\ &\quad \times \left[1 - \cos^{2N}(\varphi/2)\right]^{-1} - \frac{1}{2}\left[1 + \cos^{2N}(\varphi/2)\right] \\ &\quad \times \log_2\left[1 + \cos^{2N}(\varphi/2)\right], \\ I_F(N, \varphi) &= 1 - \frac{\pi^2}{128} - \frac{4}{9}\left[1 + \frac{\cos^{2N}(\varphi/2)}{1 + \cos^N(\varphi/2)}\right]^2 \\ &\quad + \frac{\pi^2}{128}\cos^{2N}(\varphi/2), \end{aligned} \tag{2.33}$$

where the information gain and the output fidelity are given as functions of measurement strength $\varphi \equiv g^2\tau/\Delta$ after N successive measurements.

First, we consider a single measurement $N = 1$ with one atom passing through the cavity. Both the quantifiers I_M and I_F of information gain increase monotonically with the measurement strength $\varphi \in [0, \pi]$ while the output fidelity F decreases monotonically as shown in Fig. 2.3. When $\varphi = \pi$, the QND scheme becomes a photon-number-parity measurement, as seen from Eq. (2.11) with $\frac{e^{-in\varphi} \pm 1}{2} = \frac{(-1)^n \pm 1}{2}$. Detecting the atom to be in $|e\rangle$ or $|f\rangle$ designates the cavity photon-number to be odd or even, respectively. In the case of a qubit state, this parity measurement effectively distinguishes $|0\rangle$ and $|1\rangle$. We obtain the highest information gain and the lowest fidelity when

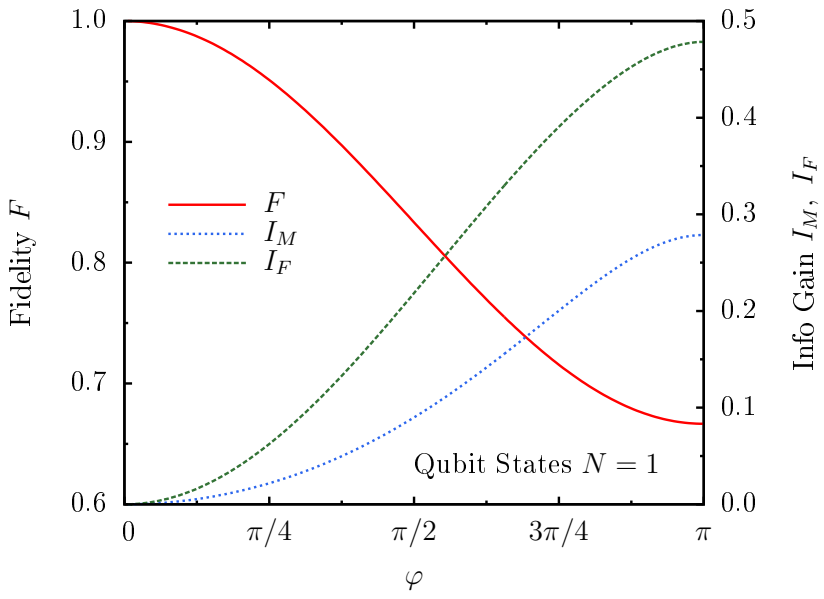

Figure 2.3: F, I_M, and I_F with respect to measurement strength φ under a single measurement on a qubit. As the measurement strength increases, the fidelity monotonically decreases while the information gain increases. When $\varphi = \pi$, the measurement discriminates the states $|0\rangle$ and $|1\rangle$ perfectly, so the largest information gain is obtained..

applying this parity measurement.

Second, we consider the case of successively performing the QND measurements many times for a given measurement strength $\varphi = g^2\tau/\Delta$. We see from Eq. (2.33) that $I_M(N, \varphi)$ and $I_F(N, \varphi)$ monotonically increase with the number N of measurements, whereas $F(N, \varphi)$ exhibit an oscillating behavior, as illustrated in Fig. 2.4. As the number N of successive measurements increases, we also see that a more information gain does not always entail a more disturbance of the state, as evidenced by the oscillating behavior with respect to N.

From Eq. (2.33), for $\varphi \neq \pi$, the limiting values of the information gain ($I_M = 1 - \frac{1}{2\ln 2} \approx 0.28$ and $I_F = 1 - \frac{4}{9} - \frac{\pi^2}{128} \approx 0.48$) and the output fidelity ($F = \frac{2}{3}$) are achieved as the number of measurements becomes increasingly large as shown in Fig. 2.4. For $\varphi = \pi$ (parity measurement), these values are achieved only with a single measurement $N = 1$. It indicates that the parity measurement extracts the most information from an unknown qubit state and leaves the state most deeply disturbed.

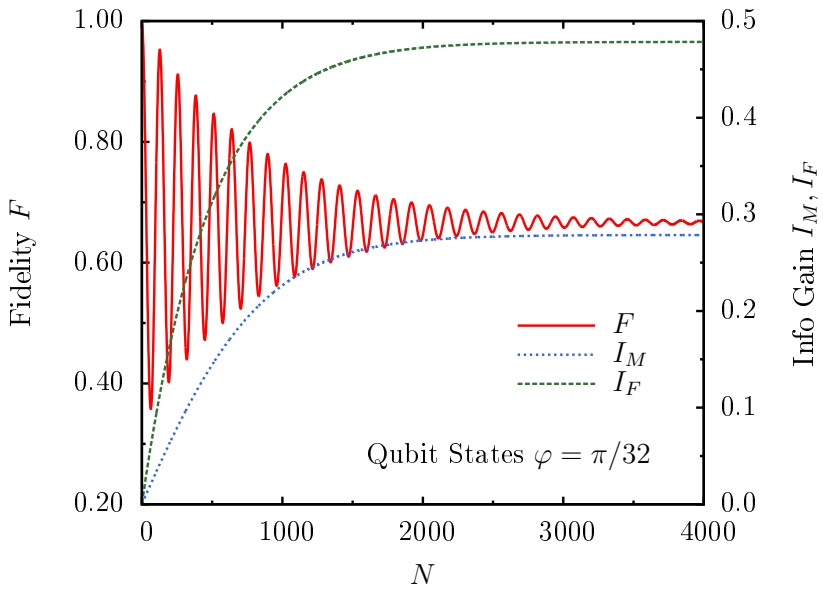

Figure 2.4: F, I_M, and I_F with respect to measurement times N under a successive measurement on a qubit with measurement strength $\varphi = \pi/32$. More measurements result in a larger information gain and a less fidelity, while the fidelity also shows an oscillating behavior.

2.2.2 Coherent states

Next we consider that the cavity field is prepared in an unknown coherent state $|\alpha\rangle \equiv ||\alpha|e^{i\beta}\rangle$ with a probability density $p(|\alpha|, \beta)$, i.e.,

$$\rho = \sum_{|\alpha|,\beta} p(|\alpha|, \beta)||\alpha|e^{i\beta}\rangle\langle|\alpha|e^{i\beta}|, \tag{2.34}$$

where a coherent state is given by

$$|\alpha\rangle = e^{-\frac{|\alpha|^2}{2}} \sum_{n=0} \frac{\alpha^n}{\sqrt{n!}}|n\rangle. \tag{2.35}$$

We assume that the coherent state of complex amplitude $\alpha = |\alpha|e^{i\beta}$ is prepared with a Gaussian distribution

$$p(|\alpha|, \beta) = \frac{1}{2\pi} \frac{1}{\sqrt{2\pi}\sigma|\alpha|} \exp\left[-\frac{(|\alpha| - |\alpha_0|)^2}{2\sigma^2}\right], \tag{2.36}$$

i.e., its magnitude $|\alpha|$ has a distribution centered at $|\alpha_0|$ with a width σ, whereas its phase β is randomly distributed over $[0, 2\pi]$. Since it is a continuous distribution, we convert the summation to an integral as

$$\sum_{|\alpha|,\beta} p(|\alpha|, \beta) \to A \int_0^\infty |\alpha| \mathrm{d}|\alpha| \int_0^{2\pi} \mathrm{d}\beta \, p(|\alpha|, \beta), \tag{2.37}$$

where A is a normalized factor.

In this case, the analytical expressions of the information gain and the fidelity are tedious to obtain, thus we study the numerical results of those quantities. As an illustration, we consider the case that the initial coherent state distribution is centered at $|\alpha_0| = 0$ with $\sigma^2 = 2$.

First, for a single measurement $N = 1$, we plot the information gain and the fidelity versus the measurement strength φ in Fig. 2.5. We observe that the fidelity decreases when the measurement strength increases, which is similar to the qubit case. At $\varphi = \pi$, the fidelity is the minimum since most elements of M_e and M_f shown in Eq. (2.11) are zero. However, the information gain at $\varphi = \pi$ is not maximum, because such a measurement can only discriminate odd or even number states, e.g. it cannot discriminate $n = 1$ or $n = 3$. From the plot we see that the maximum points are around $\pi/8$ for both kinds of information gain.

Second, we consider successive weak measurements with $\varphi = \pi/32$ for the same Gaussian distribution with $|\alpha_0| = 0$ and $\sigma^2 = 2$. As shown in Fig. 2.6, the information gain and the output fidelity behave similarly to those of the qubit case. I_M and I_F increase monotonically with the number of measurements, while the curve of fidelity exhibits a decreasing trend but with an oscillating behavior. The information gain in both forms I_M and I_F increases monotonically with respect to N for all values of φ as illustrated in Fig. 2.7.

The optimal φ_{opt} to obtain the highest information gain depends on the range of possible photon numbers. It may be ascribed to the mechanism of the QND measurements on photon numbers. It discriminates photon numbers n by a mapping from N_e to n. To accomplish this task best, it is required that n and N_e are bijective, i.e. a one-to-one correspondence between n and N_e must be established. The analytical relation is given by the conditional probability in Eq. (2.19). If the factors $c_n^2 = \sin^2(n\varphi/2)$ and $d_n^2 = \cos^2(n\varphi/2)$ are monotonous in each range of π for $n\varphi$, then

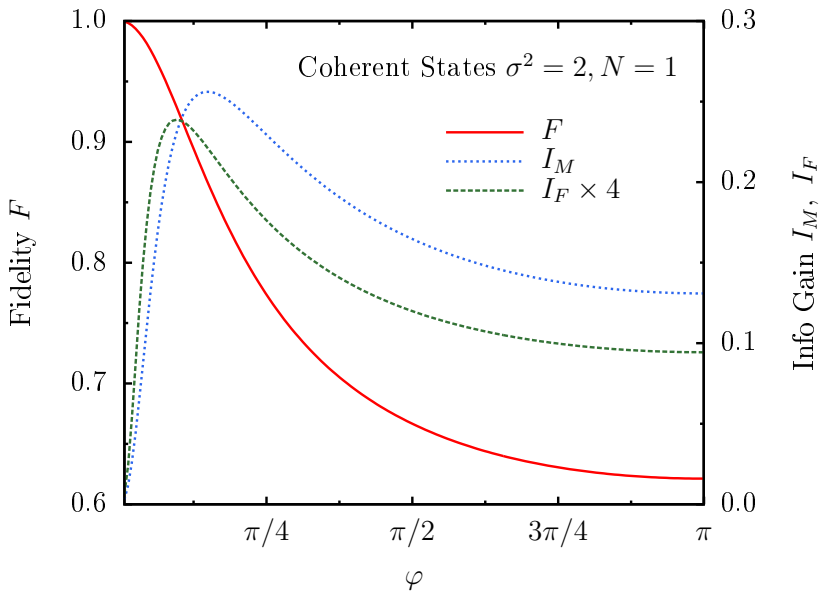

Figure 2.5: Tradeoff relation under a single measurement on coherent states ($|\alpha_0| = 0$, $\sigma^2 = 2$). I_F is multiplied by 4 for convenience of comparison.F, I_M, and I_F with respect to measurement strength φ under a single measurement. The fidelity decreases when φ increases. The peaks of I_M and I_F slightly depart from each other, however, both of them are around $\pi/8$ (b) F, I_M, and I_F with respect to measurement times N under a successive measurement on a qubit with measurement strength $\varphi = \pi/32$. More measurements result in a larger information gain and a less fidelity, while the fidelity also shows an oscillating behavior.

n and N_e are bijective. If $\varphi > \pi/(n_{\max} - n_{\min})$, we could not discriminate n perfectly, because two different n could be mapped to the same N_e. In the opposite limit, too small φ means weaker measurement, resulting in less information gain. Therefore, the optimal φ is estimated to be

$$\varphi_{\text{opt}} \approx \frac{\pi}{n_{\max} - n_{\min}} \tag{2.38}$$

This again explains why the optimal φ is π for qubit states ($n_{\max} - n_{\min} = 1$). For the prior Gaussian distribution of coherent states with zero mean and σ^2 variance, the range of $|\alpha|$ can be cut off at about $\sqrt{2}\sigma$. The photon number of the coherent state is then effectively distributed between 0 and $2\sigma^2 + 2\sigma$. Therefore the optimal measurement strength to obtain the highest information

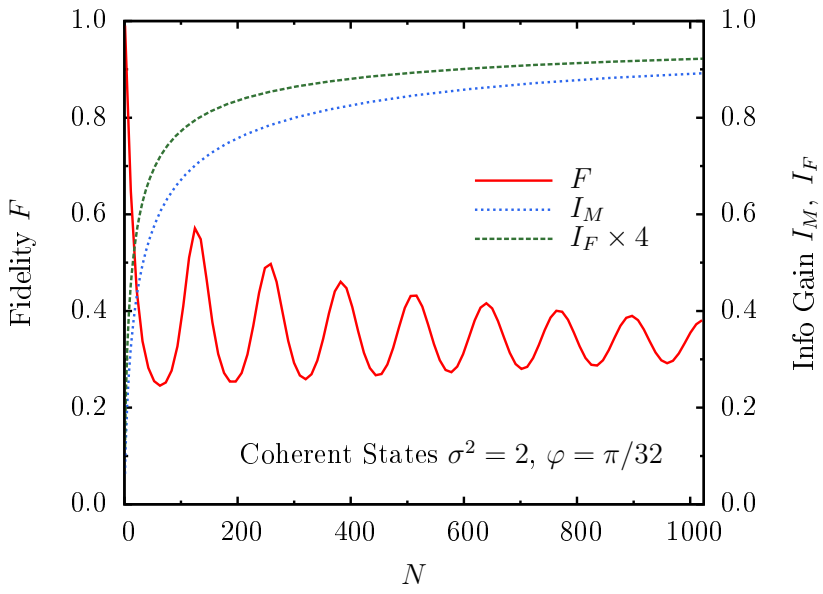

Figure 2.6: Tradeoff relation under a successive measurement on coherent states ($|\alpha_0| = 0$, $\sigma^2 = 2$). I_F is multiplied by 4 for convenience of comparison.F, I_M, and I_F with respect to measurement times N under a successive measurement when $\varphi = \pi/32$. The results are similar to those for qubit states shown in Fig. 2.4.

gain can be estimated as

$$\varphi_{\rm opt} \approx \frac{\pi}{2\sigma^2 + 2\sigma}. \tag{2.39}$$

For succussive measurements, $\varphi_{\rm opt}$ shifts a little leftward with the increase of measurement times, but is still around $\pi/(2\sigma^2 + 2\sigma)$ as shown in Fig. 2.7. To see the dependence on σ, we plot the information gains I_M and I_F after a single measurement versus φ for different σ in Fig. 2.8. We observe that with a larger σ the optimal φ becomes smaller. The analytical ansatz values are $\varphi_{\rm opt} \approx 1.3, 0.79, 0.46, 0.26$, and 0.15. The peak values for I_M are $\varphi^M_{\rm opt} \approx 1.37, 0.80, 0.47, 0.28$ and 0.16, while those for I_F are $\varphi^F_{\rm opt} \approx 0.91, 0.52, 0.30, 0.17$ and 0.10. Therefore $\varphi_{\rm opt}$ in Eq. (39) is a very good estimate of $\varphi^M_{\rm opt}$. A larger cutoff than $\sqrt{2}\sigma$ can be chosen to better fit $\varphi^F_{\rm opt}$, and the discrepancy between the peaks of I_M and I_F may be due to their different context as information measures.

Through our QND measurements, we gain informaion on which states are more probable to be the initial state. In other words, given different measurement outputs, the conditional probability

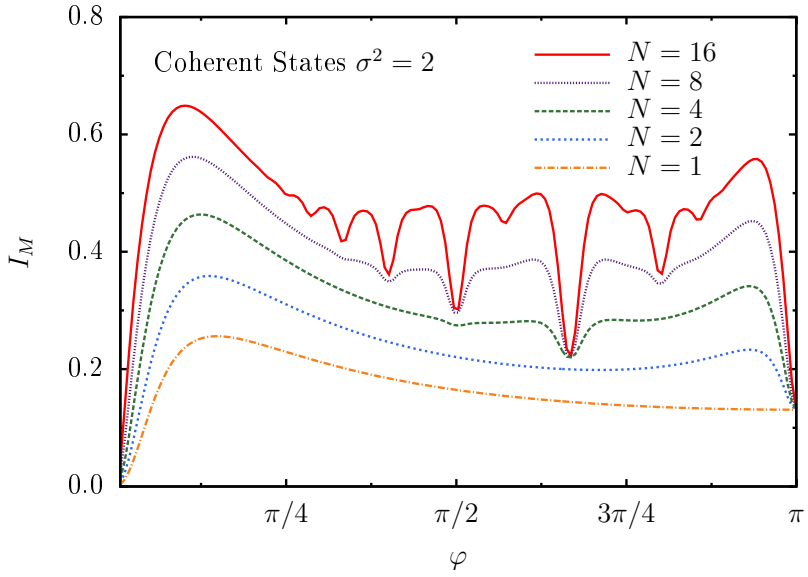

(a) Entropy of Entanglement

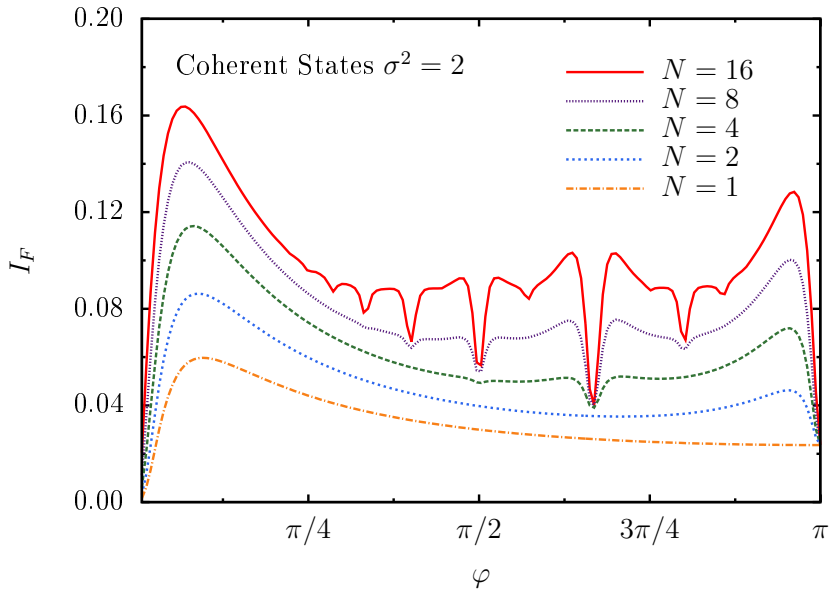

(b) Total Average Photon Numbers

Figure 2.7: Information gain I_M and I_F with respect to measurement strength φ under successive measurements with different times ($N = 1, 2, 4, 8, 16$) on coherent states ($|\alpha_0| = 0$, $\sigma^2 = 2$). The optimal values agree with results in Eq. (2.39), although they deviate slightly when N increases.

density distributions become different from, and sharper (with less Shannon entropy) than, the prior probability distribution. To see this, we plot in Fig. 2.9 the conditional probability density distributions after 8 successive weak measurements with the numerically obtained optimal $\varphi_{\rm opt}^M =$

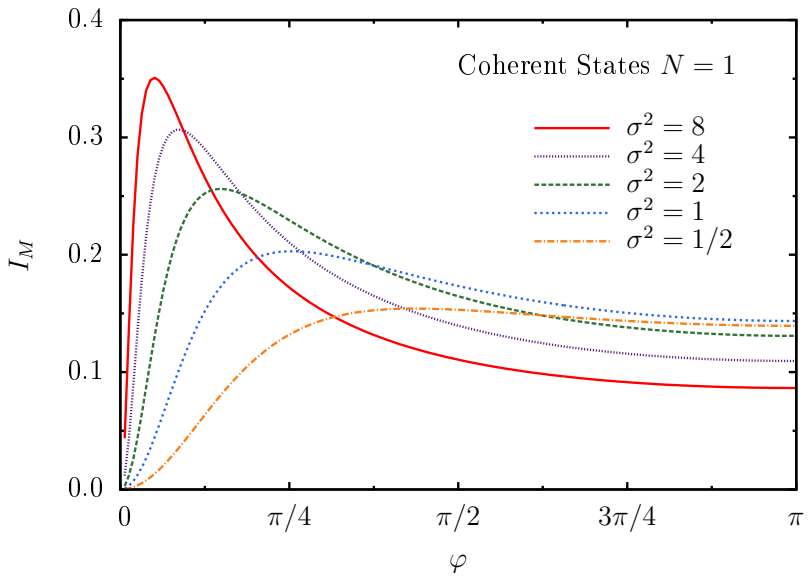

(a) Entropy of Entanglement

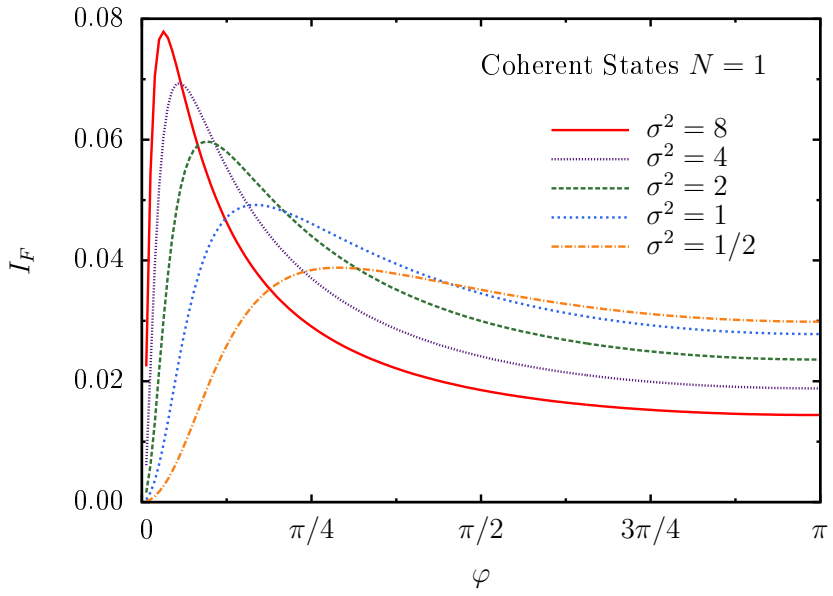

(b) Total Average Photon Numbers

Figure 2.8: Information gain I_M and I_F with respect to measurement strength φ under a single measurement on coherent states ($|\alpha_0| = 0$, different σ). As the variance σ^2 increases, the positions of peaks shift leftward. Both the peaks of I_M and I_F for the same σ are around $\pi/(2\sigma^2 + 2\sigma)$, although they slightly differ from each other.

0.3523. As a comparison, we also plot the prior probability distribution in the same figure with a solid line. We observe that these conditional curves are well separated and sharper than the prior

distribution. Each peak indicates a most probable $|\alpha|$.

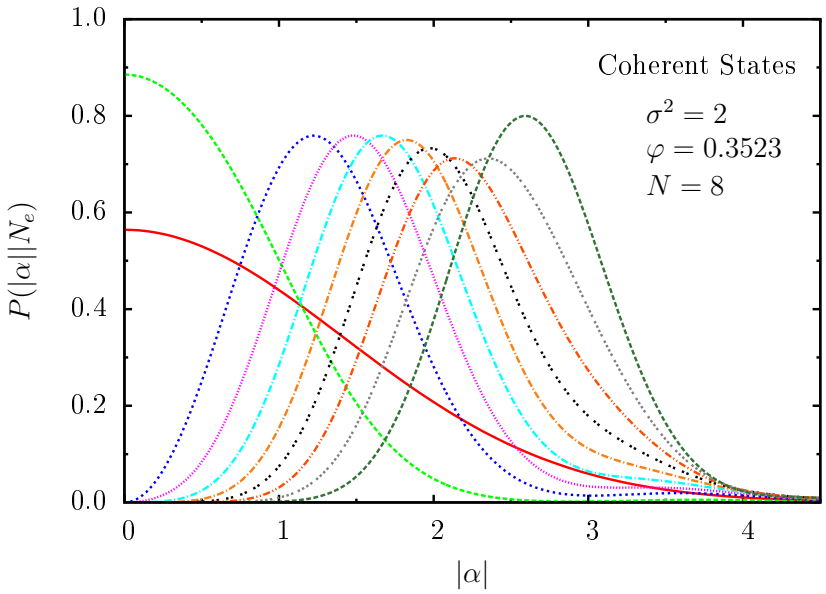

Figure 2.9: Probability density distributions when $|\alpha_0| = 0$, $\sigma^2 = 2$, $\varphi = 0.3523$ and $N = 8$. The red solid curve represents the prior distribution. The other nine curves are conditional ones given the outcomes $N_e = 0, 1, ..., 8$, from left to right. Each peak indicates a most probable $|\alpha|$.

3. INFLUENCE OF MONITORING EFFICIENCY ON STATES PROTECTION USING PARTIAL MEASUREMENT AND QUANTUM REVERSAL *

Decoherence can be caused by amplitude damping, phase damping, and depolarization. In this chapter, we focus on fighting against amplitude-damping decoherence using the three-state protection. We study how it is affected by finite monitoring efficiency. We apply the protocol to protect single-qubit states and two-qubit entangled states. We evaluate the effects of the protocol by comparing fidelity and concurrence under different conditions. We show that the protection can have either weakened positive effect or completely negative effect. We then give a criterion to decide whether to apply the protocol. An optimal strategy of setting parameters to obtain the best protection effect is also studied.

This chapter is organized as follows. In Sec. 3.1, the ideal protocol of the three-stage protection which combine partial measurement and quantum reversal is reviewed. In Sec. 3.2, the general theory of the protocol under finite monitoring efficiency is given. Then it is applied to two specific kinds of states to study its effects. In Sec. 3.3, a linear optical setup to verify our theory and results is proposed.

3.1 Ideal three-stage protection

3.1.1 Amplitude damping and its reversal

Assume that we have a two-level atom (the target system) inside a leaky cavity. Field outside (the auxiliary system) is a vacuum in zero temperature. The exited state of the atom will decay exponentially with time [96], which can be characterized by energy relaxation time T_1. Such a process is generally characterized by a quantum operation known as amplitude damping. If we only consider the state evolution of the atom, a damping process of strength d is described by a

*Reprinted with permission from "Influence of monitoring efficiency on states protection using partial measurement and quantum reversal" by Longfei Fan and M. Suhail Zubairy, Journal of Physics B 49 (23), 235504 (2016), Copyright [2016] by the IOP Publishing.

map from an input state ρ_0 to an output state ρ^{AD} [1],

$$\rho^{\mathrm{AD}} = E_0 \rho_0 E_0^\dagger + E_1 \rho_0 E_1^\dagger, \tag{3.1}$$

where the Kraus operators are given by

$$E_0(d) = \begin{pmatrix} 1 & 0 \\ 0 & \sqrt{1-d} \end{pmatrix}, \quad E_1(d) = \begin{pmatrix} 0 & \sqrt{d} \\ 0 & 0 \end{pmatrix}. \tag{3.2}$$

The damping strength depends on the time τ as $d = 1 - e^{-\tau/T_1}$. The subscript '0' indicates the outcome with no photon leaking, and vice versa. The target system collapses only when the outcome '1' is observed. Therefore this is a partially collapsed operation.

It is noticed that the operator E_0 is invertible, which means that the corresponding operation is reversible. Its inverse operator can be expressed in terms of itself and two Pauli σ_x operators [60, 53, 52],

$$E_0^{-1} = \sigma_x E_0 \sigma_x / \sqrt{1-d}. \tag{3.3}$$

If a photon is detected by the detector outside, we know the state is collapsed (the second term in Eq. (3.1)) and it will be discarded. Only the first term is allowed for further processing. We call such an operation a monitored partial measurement. Then by making two σ_x rotations in between with another monitored partial measurement, we can restore the target system as $(\sigma_x E_0 \sigma_x E_0)\rho_0(\sigma_x E_0 \sigma_x E_0)^\dagger/(1-d) \equiv \rho_0$, where the factor $1-d$ is the probability of restoring states.

3.1.2 Three-stage protection by partial measurement and quantum reversal

In the three-stage protection [59, 61, 62, 65, 63, 64], the probability amplitude of the excited state $|1\rangle$ of a target qubit is reduced by a coherent but non-unitary operation before any further processes. It makes the qubit less vulnerable to later amplitude-damping process. Applying a monitored partial measurement (E_0) can fulfill this task [59, 61, 62, 65, 63, 64], as it reduces the

probability amplitude of $|1\rangle$ by a factor of $\sqrt{1-d}$. Together with the following free amplitude damping and quantum reversal, the whole three-stage protection is shown as follows

$$\rho_0 \xrightarrow[p_\mathrm{s}]{E_0} \rho_1 \xrightarrow[d]{\mathrm{AD}} \rho_2 \xrightarrow{\sigma_x} \xrightarrow[p_\mathrm{r}]{E_0} \xrightarrow{\sigma_x} \rho_3 \tag{3.4}$$

The first stage is a monitored partial measurement with strength of p_s, which brings the qubit far away from its excited state. In the second stage, the qubit damps freely with strength of d. The third stage is a quantum reversal operation, including two σ_x rotations in between with another monitored partial measurement with strength of p_r. Assume that the input qubit state is $|\psi_0\rangle = \alpha|0\rangle + \beta|1\rangle$. If the qubit does not decay in the second damping stage, its density matrix evolves to ρ_r, which is given by

$$\begin{pmatrix} (1-p_\mathrm{r})|\alpha|^2,\ \sqrt{(1-p_\mathrm{s})(1-d)(1-p_\mathrm{r})}\alpha\beta^* \\ \sqrt{(1-p_\mathrm{s})(1-d)(1-p_\mathrm{r})}\alpha^*\beta,\ (1-p_\mathrm{s})(1-d)|\beta|^2 \end{pmatrix}. \tag{3.5}$$

Let $(1-p_\mathrm{r}) = (1-p_\mathrm{s})(1-d)$, we have $\rho_r \equiv \rho_0$ after normalization. Therefore the qubit is restored. The reversibility R is defined to be the ratio of restored qubits to all the input qubits and is given by

$$R = \mathrm{Tr}[\rho_\mathrm{r}] = (1-p_\mathrm{s})(1-d). \tag{3.6}$$

The monitored partial measurement itself is also an amplitude-damping, which makes the damping strength stronger and decreases the proportion of uncollapsed states. Therefore the reversibility is modified by a factor of $1-p_\mathrm{s}$. The success rate is defined to be the ratio of restored qubits to all the collected qubits and is given by

$$S = \frac{\mathrm{Tr}[\rho_\mathrm{r}]}{\mathrm{Tr}[\rho_3]} = \frac{1}{1+d(1-p_\mathrm{s})|\beta|^2}. \tag{3.7}$$

It is noticed that both R and S are modified by the factor of $1-p_\mathrm{s}$. As p_s increases from 0 to 1, R decreases from $1-d$ to 0. Meanwhile, S increases from $1/[1+d|\beta|^2]$ to 1. Therefore by

introducing the monitored partial measurement of strength p_s in the first stage, higher success rate is achieved at the expense of reversibility.

3.2 Three-stage protection under non-ideal monitoring

The three-stage protection depends crucially on the monitoring efficiency. Usually it is hard to reach 100% efficiency. In a recent experiment performed on superconducting circuits, the three-stage protocol is applied to protect phase qubits [65]. In this work, the monitoring operation is fulfilled as follows. First the state of a target qubit is swapped with a field state inside a resonator probabilistically. This is analogous to a leaky cavity. Then a full swap between the field state and an auxiliary qubit state is followed. If the auxiliary qubit is finally detected to be at the excited state, one can know that target qubit decays. Therefore the readout fidelity of the auxiliary qubit is equivalent to the monitoring efficiency. The readout fidelity of ground states is about 95%, and that of exited states is about 90% [65]. In the linear optical demonstration of the three-stage protection [54, 61, 62, 63, 64], once a photon is detected in the tomography stage, it must have not leaked in the previous stages. This automatically ensures 100% monitoring efficiency. However, similar detection-free methods may not be feasible for other experimental implementations straightforwardly.

Therefore it is of great necessary to study how finite monitoring efficiency influences the performance of the three-stage protection. We assume that the readout fidelity of an outcome '1' is η_1. It means that if a photon leaks, we may not observe it with a probability of $\bar{\eta}_1 = 1 - \eta_1$. Thus collapsed states can be allowed into further processes with the probability of $\bar{\eta}_1$. We also assume that the readout fidelity of an outcome '0' is η_0. It means that even if no photon leaks, we may still observe one (dark count) with a probability of $1 - \eta_0$. In a short, η_0 and η_1 determine how much proportion of uncollapsed and collapsed states is collected into further processes. Thus after a non-ideal monitored partial measurement, the states ρ_0 evolves to (without normalization)

$$\eta_0 E_0 \rho_0 E_0^\dagger + \bar{\eta}_1 E_1 \rho_0 E_1^\dagger. \tag{3.8}$$

Without loss of generality, we introduce an effective monitoring efficiency η for convenience, which is defined by

$$1-\eta=\bar{\eta}\equiv\bar{\eta}_1/\eta_0. \tag{3.9}$$

After the normalization, the state is given by

$$\rho(\bar{\eta})=\frac{1}{A}\left[E_0\rho_0E_0^\dagger+\bar{\eta}E_1\rho_0E_1^\dagger\right]. \tag{3.10}$$

where A is a normalization factor.

3.2.1 Protection of single-qubit states

Now the effective monitoring efficiency is η, the protocol of the three-stage protection shown in Eq. (3.4) should be modified to

$$\rho_0\xrightarrow[p_{\rm s},\eta]{\rm AD}\rho_1\xrightarrow[d]{\rm AD}\rho_2\xrightarrow{\sigma_x}\xrightarrow[p_{\rm r},\eta]{\rm AD}\xrightarrow{\sigma_x}\rho_3, \tag{3.11}$$

where η indicates that the state evolution in the first and the third stage is described by Eq. (3.10). E_0 above the arrows is also replaced by 'AD', because both outcomes '0' and '1' are possible if an outcome '0' is observed under non-ideal monitoring . To restore states, it is still required that $1-p_r=(1-d)(1-p)$. The final density matrix after normalization is given by

$$\rho_3=\frac{1}{A}\begin{pmatrix}|\alpha|^2+M|\beta|^2 & \alpha\beta^*\\ \alpha^*\beta & |\beta|^2+\bar{\eta}N\left[|\alpha|^2+M|\beta|^2\right]\end{pmatrix}, \tag{3.12}$$

where the factors are given by

$$\begin{aligned}M&=d(1-p_{\rm s})+\bar{\eta}p_{\rm s},\\ N&=1/[(1-d)(1-p_{\rm s})]-1,\\ A&=1+M|\beta|^2+\bar{\eta}N\left[|\alpha|^2+M|\beta|^2\right].\end{aligned} \tag{3.13}$$

The factor M can be regarded as an equivalent damping strength qualitatively. For ideal protection where $\bar{\eta} = 0$, M reduces to $d(1 - p_{\mathrm{s}})$. Damping strength d is suppressed by p_{s} as expected. For non-ideal protection where $\bar{\eta} \neq 0$, a new term $\bar{\eta} p_{\mathrm{s}}$ introduces extra damping strength. Equivalent damping strength which is larger than the original d should be avoided in practice, i.e. $M = d + (\bar{\eta} - d)p_{\mathrm{s}} < d$. Therefor $\bar{\eta} < d$ should be satisfied to get positive protection.

Next we consider some quantities which can measure the performance of the three-stage protection of a single qubit. The reversibility R is given by

$$R = \eta_0^2 \,\mathrm{Tr}\left[E_r \rho_0 E_r^\dagger\right] = \eta_0^2 (1-d)(1-p_{\mathrm{s}}), \tag{3.14}$$

where the operator $E_r = \sigma_x E_0(p_r)\sigma_x E_0(d) E_0(p_s)$. η_0^2 is introduce because of non-ideal collections happen twice in the first and the third stages. The success rate S is given by

$$S = \left[1 + M|\beta|^2 + \bar{\eta} N \left(|\alpha|^2 + M|\beta|^2\right)\right]^{-1}. \tag{3.15}$$

The output fidelity between initial states and final states is given by

$$\begin{aligned} F =& \,\mathrm{Tr}\left[\rho_0^{\frac{1}{2}} \rho_3 \rho_0^{\dagger\frac{1}{2}}\right] \\ =& \frac{1}{A}\left[1 + (M + \bar{\eta} N)|\alpha|^2|\beta|^2 + \bar{\eta} M N |\beta|^4\right] \end{aligned} \tag{3.16}$$

By setting $\bar{\eta}_0 = 0$ and $\bar{\eta}_1 = 0$, we find that the reversibility R and the success rate S reduces to the same expressions given in Sec. 3.1.2. Under finite effective monitoring efficiency, the reversibility R is modified by a factor of η_0^2 as explained above. Meanwhile, the success rate S decreases with respect to $\bar{\eta}$. This can be seen from that both M and N are non-negative and increase with respect to $\bar{\eta}$. The output fidelity of a successful restoration is 1, otherwise it is less than 1. Therefore the output fidelity should also decrease with respect to $\bar{\eta}$ as like what the success rate does. This can also be seen from its analytical expression.

To see how does the effective monitoring efficiency and other parameters affect the perfor-

mance of the three-stage protocol quantitatively, we illustrate some numerical examples for fidelity and success rate in Fig. 3.1. We find that they show rather different behavior under non-ideal efficiency compared with that under ideal efficiency. They no longer saturate the unity when p_{s} approaches 1, instead they drop to their worst values. As p_{s} becomes larger, the extra damping strength introduced by it dominates over the positive effect it has brought. This phenomenon becomes distinct especially when d itself is relatively small.

We find that there exist a critical $\bar{\eta}$ and an optimal p_{s}. When $\bar{\eta}$ is less than the critical value $\bar{\eta}_{\mathrm{c}}$, both fidelity and success rate increase monotonically in the interval from 0 to a positive $p_{\mathrm{s}}^{\mathrm{opt}}$. Meanwhile if $\bar{\eta} \geq \bar{\eta}_{\mathrm{c}}$, the fidelity and success rate decrease monotonically with respect to p_{s} in the full interval of $[0, 1]$. The optimal $p_{\mathrm{s}}^{\mathrm{opt}}$ shall be zero in such a case. Thus applying the first monitored partial measurement (setting $p_{\mathrm{s}} > 0$) has negative effect. By solving $\partial S/\partial p_{\mathrm{s}} \big|_{p_{\mathrm{s}}=0} = 0$, we obtain that

$$\bar{\eta}_{\mathrm{c}} = \frac{1}{2}\left[d - \frac{1}{d|\beta|^2} + \sqrt{\left(d - \frac{1}{d|\beta|^2}\right)^2 + 4(1-d)}\right]. \tag{3.17}$$

The values of $\bar{\eta}_{\mathrm{c}}$ under different d and $|\beta|$ are illustrated in Fig. 3.2. We notice that the protocol is able to tolerate lower monitoring efficiency under larger $|\beta|$. The reason is that amplitude damping only affects exited states. When $|\beta|$ is larger, the damping will cause more destruction, making the effect of protection more distinct. We also notice that the $\bar{\eta}_{\mathrm{c}}$ is hill-shaped with respect to damping strength d. In one hand, the positive effect of the three-stage protection dominates over its negative effect under large damping strength. In the other hand, more uncollapsed states are collected under non-ideal monitoring if the damping strength becomes larger. These two factors exert opposite influence and keep balance around $d = 0.65$, so we get a hill-shaped curve of $\bar{\eta}_{\mathrm{c}}$ with respect to d. The supremum of $\bar{\eta}_{\mathrm{c}}$ is about 0.2956, which is reached at point ($|\beta| = 1$, $d = 0.6478$). If $\bar{\eta}$ is larger than its supremum, p_{s} must be zero to avoid worse decoherence whatever $|\beta|$ and d are. Therefore a small enough value of $\bar{\eta}$ is required to get positive protection effect for most conditions.

When the above critical condition for the effective monitoring efficiency is satisfied, a positive

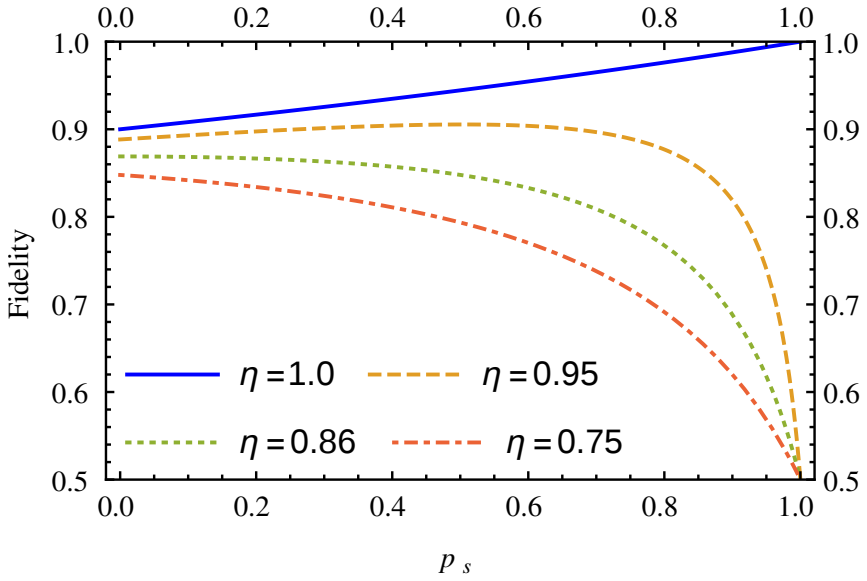

(a) g con eta 00

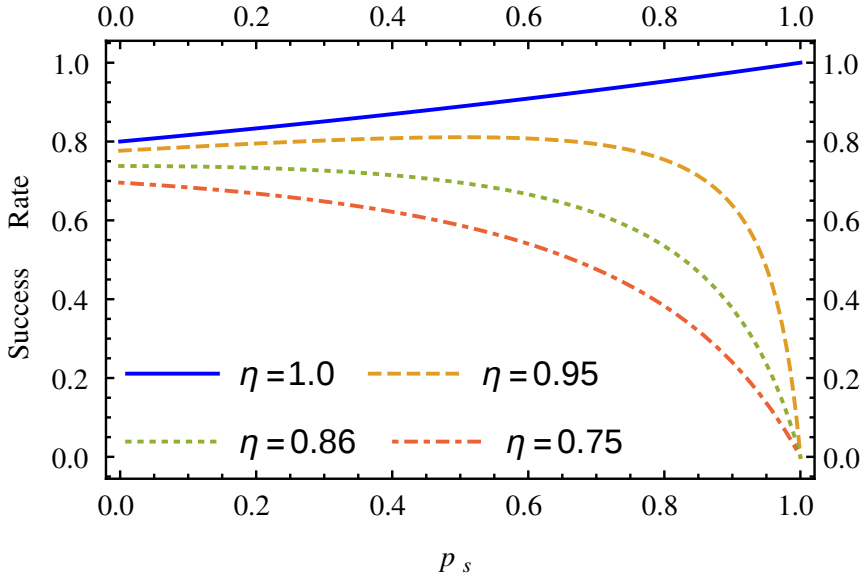

(b) g con bg 01

Figure 3.1: Fidelity and success rate with respect to p_{s} under different effective monitoring efficiency in the three-stage protection of a single-qubit state initially prepared at $|\varphi\rangle = (|0\rangle+|1\rangle)/\sqrt{2}$. The damping strength $d = 0.5$, and the corresponding $\bar{\eta}_{\mathrm{c}} = 0.14$. The fidelity and success rate do not increase monotonically with respect to p_s in the full interval of $[0, 1]$ as like in the ideal case (solid line). When the effective monitoring efficiency is greater than the critical value, they decrease after optimal points and finally reach their minimum values. Under the critical value $\eta < 1 - \bar{\eta}_{\mathrm{c}} = 0.86$, they decrease monotonically in the full interval of $[0, 1]$.

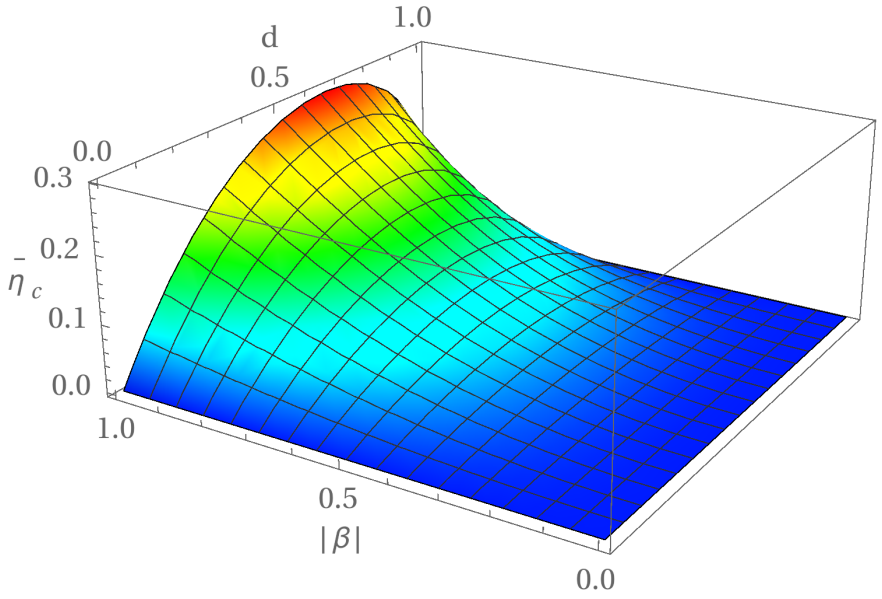

Figure 3.2: Critical value $\bar{\eta}_{\rm c}$ with respect to different amplitude-damping strength d and probability amplitude $|\beta|$. The supremum of $\bar{\eta}_{\rm c}$ is about 0.2956, which is reached when $|\beta| = 1, d = 0.6478$.

optimal $p_{\rm s}^{\rm opt}$ is possible. By solving $\partial S/\partial p_{\rm s} = 0$, we give that

$$p_{\rm s}^{\rm opt} = 1 - \sqrt{\frac{\bar{\eta}\left(1-\eta|\beta|^2\right)}{\eta|\beta|^2(1-d)(d-\bar{\eta})}}. \tag{3.18}$$

In the denominator, it seems that the term $d - \bar{\eta}$ may be negative and cause an irrational result. However in the previous discussion of the equivalent damping strength M in Eq. (3.13), we have already pointed out qualitatively that the condition $\bar{\eta} < d$ should be satisfied. We have also proved strictly that $\bar{\eta} < \bar{\eta}_{\rm c} < d$ using the expression for $\bar{\eta}_{\rm c}$, which gives a stronger and tighter condition than $\bar{\eta} < d$. The proof is straightforward, so we omit it here. In Fig. 3.3, we illustrate some numerical curves of $p_{\rm s}^{\rm opt}$ with respect to the effective monitoring efficiency under different damping strength. We set $|\beta|^2 = 0.5$ for the initial state. With damping strength fixed, the optimal $p_{\rm s}$ decreases from 1 to 0 as $\bar{\eta}$ increases from 0 to its critical value. Beyond the critical value, $p_{\rm s}^{\rm opt}$ should always be zero. The intersections of the curves and the x-axis are just the critical values of $\bar{\eta}$. Actually, by solving $p_{\rm s}^{\rm opt} = 0$, we can reproduce the result in Eq. (3.17).

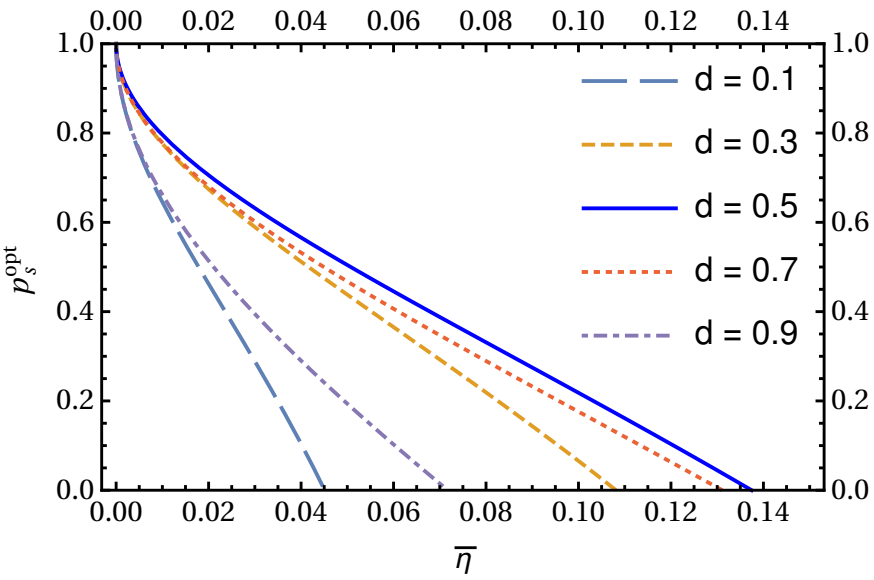

Figure 3.3: Optimal p_{s} of obtaining the best success rate with respect to the effective efficiency $\bar{\eta}$ under different damping strength d. We set $|\beta|^2 = 0.5$ for initial states. $p_{\mathrm{s}}^{\mathrm{opt}}$ decreases from 1 to 0 as $\bar{\eta}$ increase from 0 to its critical value. And beyond the critical value, $p_{\mathrm{s}}^{\mathrm{opt}}$ keeps zero.

3.2.2 Protection of two-qubit entangled states

Next we consider the influence of the non-ideal monitoring on the protection of two-qubit entangled states. The three-stage protection of such states has been demonstrated experimentally in linear optical system [62] under ideal monitoring efficiency. A general two-qubit state is described by

$$|\varphi\rangle = \alpha\,|00\rangle + \beta\,|01\rangle + \gamma\,|10\rangle + \delta\,|11\rangle\,. \tag{3.19}$$

And $\rho_0 = |\varphi\rangle\langle\varphi|$. The dynamics of entanglement has been investigated in details for the state $\alpha\,|00\rangle + \delta\,|11\rangle$ [97]. We assume that there occurs amplitude damping for both qubits locally and independently. Therefore the amplitude-damping process for the whole system can be described by four Kraus operators as follows

$$\begin{aligned} \rho^{\mathrm{AD}} &= \sum_{i,j=0,1} E_{ij}\rho_0 E_{ij}^{\dagger}, \\ E_{ij}(p_1,p_2) &= E_i(p_1)\otimes E_j(p_2),\ i,j=0,1. \end{aligned} \tag{3.20}$$

If the effective monitoring efficiency η is less than 1 and no photons are detected, the state collapses partially to a mixed state given by

$$\rho_{\bar{\eta}}^{\mathrm{AD}} = \sum_{i,j=0,1} \bar{\eta}^{i+j} E_{ij} \rho_0 E_{ij}^{\dagger}. \tag{3.21}$$

These two qubits undergo the three-stage protection locally and independently shown as follows

$$\rho_0 \xrightarrow[p_{\mathrm{s}1},p_{\mathrm{s}2};\ \eta]{\mathrm{AD}} \rho_1 \xrightarrow[d_1,d_2]{\mathrm{AD}} \rho_2 \xrightarrow{\sigma_x} \xrightarrow[p_{\mathrm{r}1},p_{\mathrm{r}2};\ \eta]{\mathrm{AD}} \xrightarrow{\sigma_x} \rho_3. \tag{3.22}$$

For simplicity, we set $p_{\mathrm{s}1} = p_{\mathrm{s}2} = p_{\mathrm{s}}$, $d_1 = d_2 = d$, and $p_{\mathrm{r}1} = p_{\mathrm{r}2} = p_{\mathrm{r}}$. Again, we ensure the requirement for successful reversal that $1 - p_{\mathrm{r}} = (1-d)(1-p_{\mathrm{s}})$.

Now we consider two specific entangled systems. Firstly, if the initial state is prepared at

$$\rho_0^{\beta\gamma} = (\beta\,|01\rangle + \gamma\,|10\rangle)(\beta^*\,\langle 01| + \gamma^*\,\langle 10|), \tag{3.23}$$

then it finally evolves to the following state according to the procedure shown in Eq. (3.22),

$$\rho_3^{\beta\gamma} = \frac{1}{A_1} \begin{pmatrix} e_1 & 0 & 0 & 0 \\ 0 & a_1 & b_1 & 0 \\ 0 & b_1^* & c_1 & 0 \\ 0 & 0 & 0 & f_1 \end{pmatrix}, \tag{3.24}$$

where the factors are given by

$$\begin{aligned} a_1 &= |\beta|^2 + \bar{\eta}MN, \;\; b_1 = \beta\gamma^*, \\ c_1 &= |\gamma|^2 + \bar{\eta}MN, \\ e_1 &= M, \;\; f_1 = \bar{\eta}N(1+\bar{\eta}MN), \\ A_1 &= M + (1+\bar{\eta}N)(1+\bar{\eta}MN). \end{aligned} \tag{3.25}$$

The factors M and N have been given in Eq. (3.13). Secondly if the initial state is prepared at

$$\rho_0^{\alpha\delta} = (\alpha\,|00\rangle + \delta\,|11\rangle)(\alpha^*\,\langle 00| + \delta^*\,\langle 11|), \tag{3.26}$$

then it finally evolves to

$$\rho_3^{\alpha\delta} = \frac{1}{A_2}\begin{pmatrix} a_2 & 0 & 0 & b_2 \\ 0 & e_2 & 0 & 0 \\ 0 & 0 & f_2 & 0 \\ b_2^* & 0 & 0 & c_2 \end{pmatrix}, \tag{3.27}$$

where the factors are given by

$$\begin{aligned} a_2 &= |\alpha|^2 + M^2|\delta|^2,\ \ b_2 = \alpha\delta^*, \\ c_2 &= \bar{\eta}^2N^2|\alpha|^2 + (1+\bar{\eta}MN)^2|\delta|^2, \\ e_2 &= f_2 = \bar{\eta}N\left(|\alpha|^2 + M^2|\delta|^2\right) + M|\delta|^2, \\ A_2 &= (1+\bar{\eta}N)^2|\alpha|^2 + (1+M+\bar{\eta}MN)^2|\delta|^2. \end{aligned} \tag{3.28}$$

To evaluate the performance of the three-stage protection on entangled states, we utilize the concurrence as a measure of entanglement, which is defined by [98]

$$C(\rho) = \mathrm{Max}\left\{0,\ \sqrt{\lambda_1} - \sqrt{\lambda_2} - \sqrt{\lambda_3} - \sqrt{\lambda_4}\right\}. \tag{3.29}$$

The quantities $\lambda_1, \ldots, \lambda_4$ are the eigenvalues of $\rho(\sigma_y \otimes \sigma_y)\rho^*(\sigma_y \otimes \sigma_y)$ in decreasing order, where σ_y is the Pauli-y operator. The concurrence of an arbitrary two-qubits state is $C = |\alpha\beta - \gamma\delta|$. For a damping two-qubit state without any protection, concurrence becomes [99]

$$C(d) = \mathrm{Max}\left\{0,\ 2(1-d)(|\alpha\delta - \gamma\beta| - d|\delta|^2)\right\}. \tag{3.30}$$

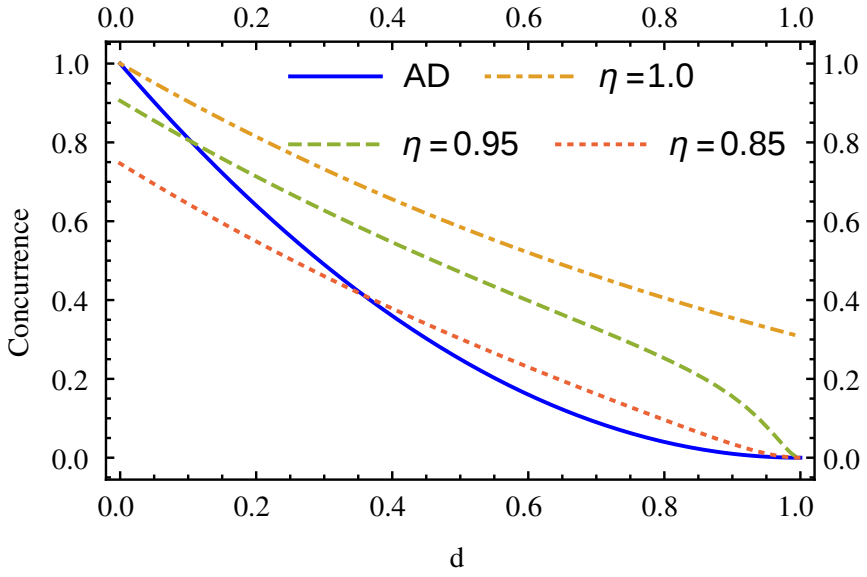

(a) g con eta 00

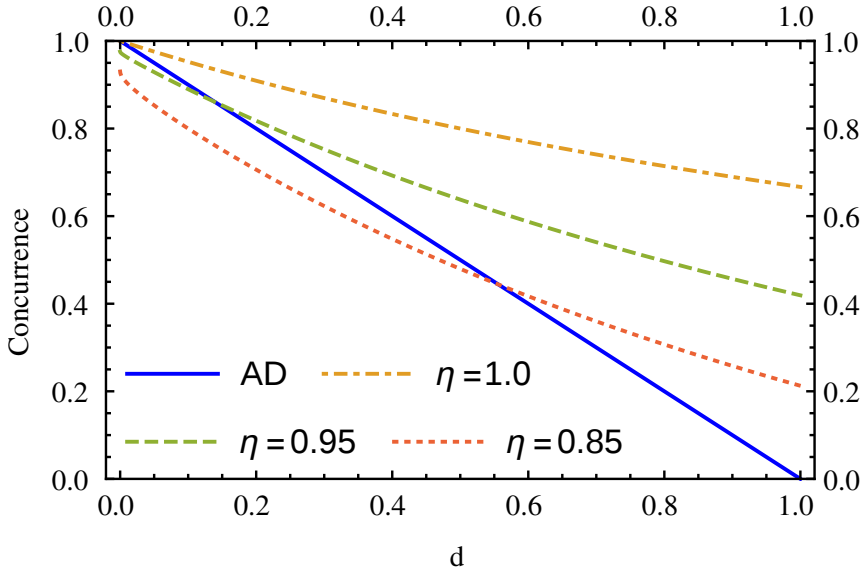

(b) g con bg 01

Figure 3.4: Concurrence with respect to damping strength d in the protection of two-qubit entangled states (a) $|\varphi_0\rangle = (|00\rangle + |11\rangle)/\sqrt{2}$ and (b) $|\varphi_0\rangle = (|01\rangle + |10\rangle)/\sqrt{2}$ under different effective efficiency η. The solid blue line shows the result for states that undergo free amplitude damping alone. For the rest curves, the three-stage protection protocol is applied and we set $p_s = 0.5$. The protocol still works to recover the concurrence under larger d, but whose effects suffers a lot when the efficiency is non-ideal. Under smaller damping strength d and lower efficiency η, the protocol fails to protect the entanglement.

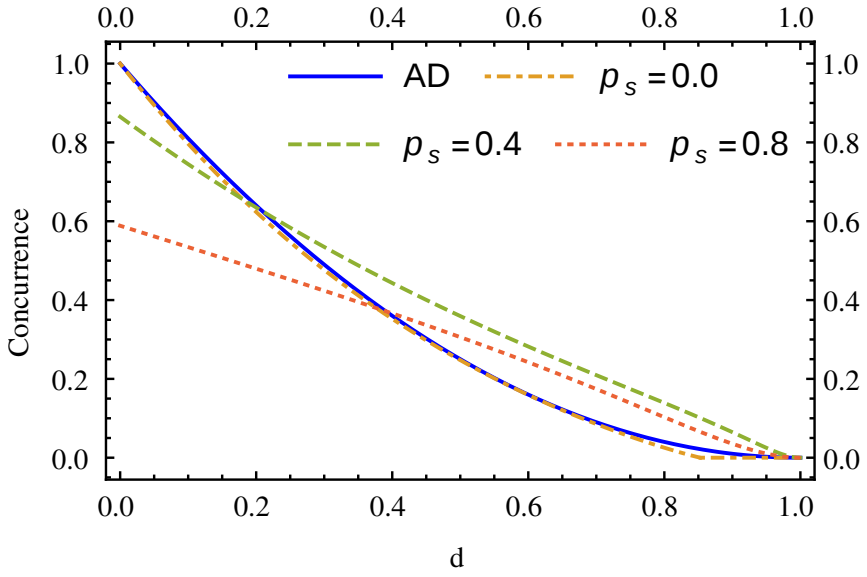

(a) g con eta 00

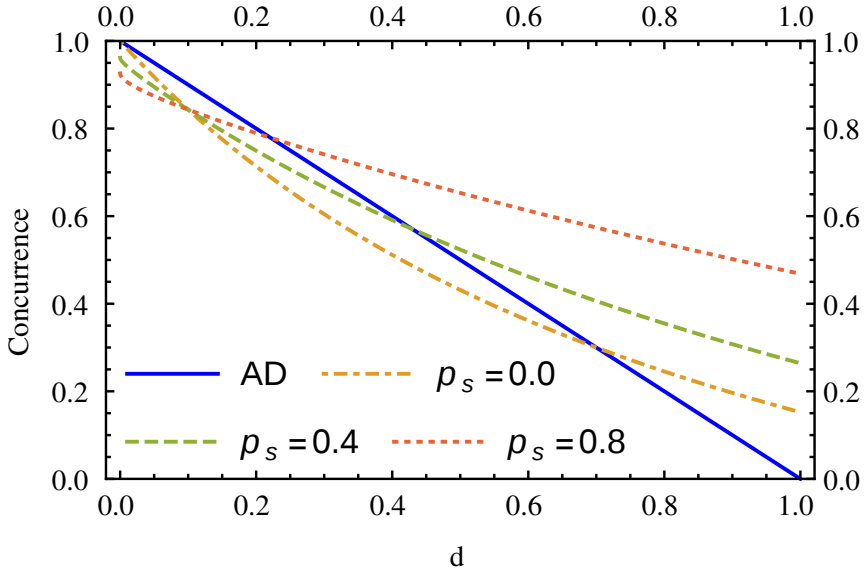

(b) g con bg 01

Figure 3.5: Concurrence with respect to damping strength d in the protection of two-qubit entangled states (a) $|\varphi_0\rangle = (|00\rangle + |11\rangle)/\sqrt{2}$ and (b) $|\varphi_0\rangle = (|01\rangle + |10\rangle)/\sqrt{2}$ under different p_s. The solid blue line shows the result for states that undergo free amplitude damping alone. For the rest curves, the three-stage protection protocol is applied and we set $\eta = 0.9$. It is shown that the protocol still work to recover the entanglement when the detection efficiency is non-ideal, especially for larger d. However, under smaller d and larger p_s, the 'protection' makes concurrence worse.

The concurrence of the states $\rho_3^{\beta\gamma}$ and $\rho_3^{\alpha\delta}$ are given by

$$
\begin{aligned}
C_{\beta\gamma} &= \mathrm{Max}\left\{0,\ 2\frac{|\beta||\gamma| - \sqrt{\bar{\eta}MN(1+\bar{\eta}MN)}}{M+(1+\bar{\eta}N)(1+\bar{\eta}MN)}\right\}, \\
C_{\alpha\delta} &= \mathrm{Max}\left\{0,\ 2\frac{|\alpha||\delta| - M|\delta|^2 - \bar{\eta}N\left(|\alpha|^2 + M^2|\delta|^2\right)}{(1+\bar{\eta}N)^2|\alpha|^2 + (1+M+\bar{\eta}MN)^2|\delta|^2}\right\}.
\end{aligned}
\tag{3.31}
$$

Some numerical results are illustrated in Fig. 3.4 and Fig. 3.5. It shows that, under certain conditions, the three-stage protocol helps recover the change of concurrence caused by amplitude damping. However when the effective monitoring efficiency is less than 100%, the effect of the protocol is weakened distinctly. The results can be even worse than that given in Eq. (3.30), especially when the strength d itself is small. The cross points of the solid blue curve with the other curves give the critical value of d. Lower efficiency η and larger p_{s} result in a greater critical value. If d is less than its critical value, it is better to abandon the monitored partial measurement applied in the first-stage. Because it brings more destructive effect than protective effect due to the extra amplitude-damping strength it introduces.

3.3 A proposal for experimental verification

To experimentally verify our theory on the three-stage protection under non-ideal monitoring, a continuously varied effective efficiency is necessary. We can modify the superconducting circuits experiment [65] by intentionally accepting some collapsed states to lower the monitoring efficiency. However the efficiency cannot reach 100%, since the maximum readout fidelity is only about 90%. Furthermore some other decoherence sources are difficult to be isolated. To see the influence of effective monitoring efficiency exclusively, we can implement the linear optical setup proposed by Q. Sun, *et al.* [54] with a few modifications. Even though the amplitude damping in this setup is intentionally generated, it is a good experimental platform for studying the performance of three-stage protection because of its well controllability [61, 62, 63, 64]. The parameters like damping strength and the effective monitoring efficiency can be adjusted to any necessary values to fulfill a complete test.

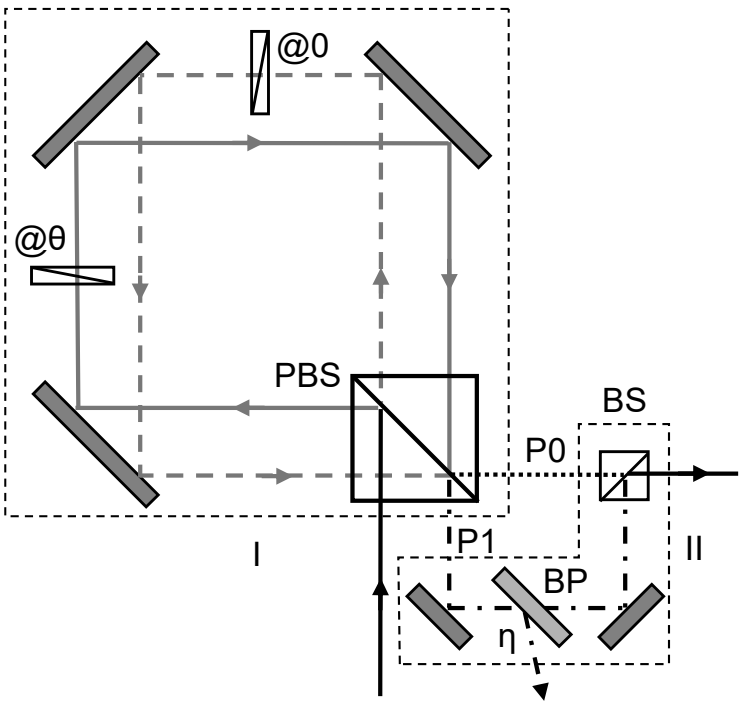

Figure 3.6: The proposed experimental set-up for demonstrating non-ideal monitored partial measurement. Part I is a Sagnac-like interferometer composed of one polarization beam splitter (PBS), three mirrors, and two half-wave plates (HWP). The strength of amplitude damping is controlled by angle value θ. The two outputs of Part I, P0 and P1, will be incoherently mixed at the beam splitter (BS), as the difference of path-length is set to be sufficiently larger than the coherent length of a single photon. A set of Brewster-angle plates is inserted to reflect out the horizontally polarized photons in path P1 with a probability of η. Setting $\eta = 0$, we get free amplitude damping. Otherwise we get non-ideally monitored partial measurement. Removing path P1 (setting $\eta = 1$ equivalently), we get ideally monitored amplitude damping since all collapsed states are discarded.

The modified setup is illustrated in Fig. 3.6. Input photons are prepared at a superposition of polarized photonic state $\alpha |H\rangle + \beta |V\rangle$. We regard $|H\rangle$ as $|0\rangle$ and $|V\rangle$ as $|1\rangle$. The horizontally polarized photon goes through the interferometer for phase matching, and is transmitted into P0 when it comes back to the PBS. The vertically polarized photon is reflected by the polarizing beam splitter (PBS) and then rotated by the half-wave plate (HWP) by an angle of θ. It corresponds to the map, $|1\rangle \rightarrow \cos(2\theta) |1\rangle + \sin(2\theta) |0\rangle$. When it comes back to the PBS, $\cos(2\theta) |1\rangle$ is reflected into P0 and $\sin(2\theta) |0\rangle$ is transmitted into P1. The angle value θ controls the amplitude-damping strength as $d = \sin^2(2\theta)$. At P0, the photons are coherently superposed to $|0\rangle + \cos(2\theta) |1\rangle$, meanwhile at P1, we get $\sin(2\theta) |0\rangle$. The length difference of P0 and P1 is intentionally set to be sufficiently larger than the coherent length ($\sim 140\mu m$ for a typical linear optical setup) of a single photon, so they will be mixed incoherently by the beam splitter (BS). Finally we obtain the amplitude-damping state given in Eq. (3.1).

In additional to the above setup, we insert a set of Brewster-angle plates in the path P1. It reflects out and thus discards the horizontally polarized photons in the path P1 with a probability of η, which is just the effective monitoring efficiency. Therefore we obtain the modified state described in Eq. (3.10). Taking off P1 and collecting the output P0 exclusively, we can implement an ideal monitored partial measurement. In summary, by adjusting Part II, we can implement free amplitude damping, ideally and non-ideally monitored partial measurement. Using another two HWPs to implement σ_x rotations, we have all the key elements required for the three-stage protection. Preparation and tomography of states can also be implemented using common methods.

4. QUANTUM ILLUMINATION USING NON-GAUSSIAN STATES GENERATED BY PHOTON SUBTRACTION AND PHOTON ADDITION *

In this chapter, we apply various two-mode entangled states to quantum illumination, particularly the non-Gaussian states obtained by photon subtraction and photon addition. We then study error probability of each state with respect to squeezing strength and signal strength of the detecting states respectively. The performance is evaluated by the Helstrom limit [100] and the quantum Chernoff bound [101]. The entanglement strength is measured by von Neumann entropy of reduced density operators. We show that under the same squeezing strength, non-Gaussian states can enhance quantum illumination because of larger entanglement and signal strength. However, TMSS performs better than other non-Gaussian states if the comparison is made under the same signal strength. We also show that the ratios of photons allocated between each mode of the two-mode entangled states also affect the performance of quantum illumination, even when entanglement strength is the same.

This chapter is organized as follows. In Sec. 4.1.1, we give a brief review of quantum illumination and its equivalent model. In Sec. 4.1.2, we introduce various non-Gaussian states and discuss their properties. In Sec. 4.2 we compare their performance in quantum illumination under different conditions. In Sec. 4.3, we study the performance of asymmetrical two-mode entangled states.

4.1 Quantum illumination and non-Gaussian states

4.1.1 Quantum illumination

The task of quantum illumination is to determine the existence of a low-reflective object which is embedded in a noisy thermal bath. Its equivalent model is illustrated in Fig. 4.1. The two-mode entangled photon state ρ_{AB} is used as the detecting state. The mode B (signal) is sent for detecting the suspect object, i.e. it can be reflected back by the object if there presents one. The mode A

*Reprinted with permission from "Quantum illumination using non-Gaussian states generated by photon subtraction and photon addition" by Longfei Fan and M. Suhail Zubairy, Phys. Rev. A 98, 012319 (2018), Copyright [2018] by the American Physical Society.

(idler) is retained to be measured together with the returned signal B'. The suspect object can be modeled by a beam splitter with low reflectance R. The thermal noise C, whose average photon number is N_{th}, will enter the final measurement device M if no object is present. If an object is present, the thermal noise is mixed with B by the beam splitter. In the latter, the average photon number of the thermal noise is adjusted to be $N'_{\text{th}} = \frac{N_{\text{th}}}{1-R}$ to make compensation for the loss during mixing.

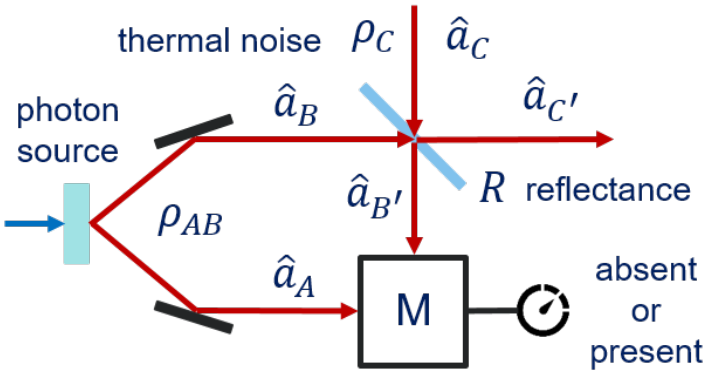

Figure 4.1: Model of quantum illumination

Let the creation operators for the idler, the signal, and the thermal noise be a_A, a_B, and a_C. The output modes are labeled by $a_{B'}$ and $a_{C'}$ as shown in Fig 4.1. The two-mode mixing operator $U(\xi) = \exp\left(\xi a_B^\dagger a_C - \xi^* a_B a_C^\dagger\right)$ describes the beam splitter, where $\xi = \arcsin\sqrt{R}$. Thus we have $a_{B'} = \cos(\xi)a_C - \sin(\xi)a_B$. Two possible output states ρ_0 and ρ_1 can enter the measurement device M, depending on whether the suspect object is absent or present.

$$\begin{aligned} \text{Object absent} : \rho_0 &= \text{Tr}_B[\rho_{AB}] \otimes \rho_C, \\ \text{Object present} : \rho_1 &= \text{Tr}_C[U\rho_{AB} \otimes \rho_C U^\dagger]. \end{aligned} \tag{4.1}$$

Now the measurement device M has to infer whether an object is present or not by discriminating above two states. The performance of discrimination can be measured by the error probability

of inference. Here we suppose that the suspect object is equally absent and present. If we have N identical copies of entangled states for detection, the optimal error probability is given by the Helstrom limit [100]

$$P_{\mathrm{err},N} = \frac{1}{2}\left(1 - \frac{1}{2}\left\|\rho_0^{\otimes N} - \rho_1^{\otimes N}\right\|\right). \tag{4.2}$$

It is usually hard to be evaluated because of the high dimensionality. Another difficulty is that it is not monotonic for the tensor power. An asymptotically tight upper bound, which is called the quantum Chernoff bound (QCB) [101], is easier to evaluate and is given by

$$P_{err,N} \leq \frac{1}{2}P_{\mathrm{QCB}}^{N} = \frac{1}{2}\left\{\min_{0\leq t\leq 1} \mathrm{Tr}\left[\rho_0^t\, \rho_1^{1-t}\right]\right\}^N. \tag{4.3}$$

We will use the above two quantities to measure of performance of quantum illumination. Meantime the entanglement of a detecting state can be measured by von Neumann entropy of reduced density operators, which is given by

$$E(|\psi_{\mathrm{AB}}\rangle) = -\,\mathrm{Tr}[\rho_{\mathrm{A}} \ln \rho_{\mathrm{A}}] = -\,\mathrm{Tr}[\rho_{\mathrm{B}} \ln \rho_{\mathrm{B}}], \tag{4.4}$$

where the reduced density operators $\rho_{\mathrm{A}} = \mathrm{Tr}_{\mathrm{B}}\,|\psi_{\mathrm{AB}}\rangle\langle\psi_{\mathrm{AB}}|$ and $\rho_{\mathrm{B}} = \mathrm{Tr}_{\mathrm{A}}\,|\psi_{\mathrm{AB}}\rangle\langle\psi_{\mathrm{AB}}|$. We will use the term 'entropy of entanglement' and the label E for it in remaining parts of our manuscript.

4.1.2 Non-Gaussian entangled states

Two-mode squeezed state (TMSS) is a widely used entanglement state in continuous-variable quantum information [102, 103]. It is a Gaussian state and is given by

$$|\mathrm{TMSS}\rangle = \sqrt{1-\lambda^2}\sum_{n=0}^{\infty}\lambda^n\,|n\rangle\,|n\rangle\,, \tag{4.5}$$

where $\lambda = \tanh s$ and s is the squeezing parameter. Quantum illumination has been realized experimentally with TMSS as the entangled detecting photon source [80, 104, 105, 106, 107]. As entanglement is regarded as the key quantum resource of quantum illumination, we expect that

detecting states with enhanced entanglement can achieve lower error probability.

A combination of photon-subtraction and photon-addition operations can generate various non-Gaussian entangled states which have enhanced entanglement [76, 77]. Here we will study photon-subtraction (PS), photon-addition (PA), photon-subtraction-following-addition (PSA), and photon-addition-following-subtraction (PAS) states. It has also been shown that a coherent superposition of both photon subtraction and photon addition [83] leads to the strongest enhancement of entanglement under small squeezing strength [84]. We call the non-Gaussian state generated by such an operation a 'PCS' state for short. The former four kind of states are given by

$$\begin{aligned}
\hat{a}\hat{b}\left|\mathrm{TMSS}\right\rangle &\doteq \sqrt{A_1}\sum_{n=0}^{\infty}(n+1)\lambda^n\left|n\right\rangle\left|n\right\rangle, \\
\hat{a^\dagger}\hat{b^\dagger}\left|\mathrm{TMSS}\right\rangle &\doteq \sqrt{A_1}\sum_{n=0}^{\infty}(n+1)\lambda^n\left|n+1\right\rangle\left|n+1\right\rangle, \\
\hat{a}\hat{a}^\dagger\hat{b}\hat{b}^\dagger\left|\mathrm{TMSS}\right\rangle &\doteq \sqrt{A_2}\sum_{n=0}^{\infty}(n+1)^2\lambda^n\left|n\right\rangle\left|n\right\rangle, \\
\hat{a}^\dagger\hat{a}\hat{b}^\dagger\hat{b}\left|\mathrm{TMSS}\right\rangle &\doteq \sqrt{A_2}\sum_{n=0}^{\infty}(n+1)^2\lambda^n\left|n+1\right\rangle\left|n+1\right\rangle,
\end{aligned} \tag{4.6}$$

where the $\doteq$ means that left-hand side equal right-hand side after normalization. The normalization factors are given by

$$A_1 = \frac{(1-\lambda^2)^3}{1+\lambda^2},\ A_2 = \frac{(1-\lambda^2)^5}{1+11\lambda^2+11\lambda^4+\lambda^6}. \tag{4.7}$$

The PCS state is given by [84]

$$\begin{aligned}
&\left(t_a\hat{a}+r_a\hat{a}^\dagger\right)\left(t_b\hat{b}+r_b\hat{b}^\dagger\right)\left|\mathrm{TMSS}\right\rangle \\
&\doteq \sqrt{A_3}\sum_{n=0}^{\infty}\lambda^n\Big[\lambda t_a t_b(n+1)\left|n\right\rangle\left|n\right\rangle \\
&\quad+\lambda t_a r_b\sqrt{(n+1)(n+2)}\left|n\right\rangle\left|n+2\right\rangle \\
&\quad+\lambda r_a t_b\sqrt{(n+1)(n+2)}\left|n+2\right\rangle\left|n\right\rangle \\
&\quad+r_a r_b(n+1)\left|n+1\right\rangle\left|n+1\right\rangle\Big],
\end{aligned} \tag{4.8}$$

where $t_i^2 + r_i^2 = 1$ $(i = a,\ b)$ and the normalization factor is given by

$$A_3 = \frac{(1-\lambda^2)^3}{\lambda^2(1+|t_a r_b^* + r_a t_b^*|) + |t_a t_b \lambda^2 + r_a r_b|^2}. \tag{4.9}$$

Some properties of these non-Gaussian states have been discussed in previous study [77, 84]. However, the previous discussion on PCS states is limited to symmetrical ones, where $r_a = r_b$ holds. Here we discuss these states with a focus on their entanglement and photon numbers, particularly for asymmetrical PCS states. We illustrate the entropy of entanglement E in Fig. 4.2a and the total average photon number $\langle n \rangle$ in Fig. 4.2b for each state with respect to λ. It is shown that for a given λ, PS and PA have the same entropy of entanglement E, however, PA has one more photon per mode than that of PS. Similar results are observed for PSA and PAS. Meanwhile PSA (PAS) has larger entanglement than PS (PA). Therefore, non-Gaussian operations not only enhance entanglement, but also bring larger average photon numbers, i.e., signal strength.

The properties of PCS are somehow complicated because of free choices on r_a and r_b. In Fig. 4.2, for each λ, we choose the pair of r_a and r_b which leads to the largest entropy of entanglement E for plotting. With such choices, the PCS state has the most enhanced entanglement than any other state under small squeezing strength where $\lambda \lessapprox 0.15$ as shown in Fig. 4.2a. In region from $\lambda \approx 0.15$ to $\lambda \approx 0.35$, its entanglement becomes less than that of PAS and PSA, but still larger than entanglement of others. When $\lambda \gtrapprox 0.35$, the optimal PCS reduces to PA or PS. That is to say, there are two optimal choices which lead to the largest entanglement: $r_a = r_b = 0$ and $r_a = r_b = 1$. In Fig. 4.2b, The curve of PCS start from point $(0, 1.0)$, then it goes between those of PS and PA until the point $\lambda \approx 0.05$. For λ from 0.05 to 0.35, the curve of PCS almost overlaps with that of PA ($r_a = r_b = 1$). Our numerical results show that values of r_a and r_b are very close to 1.0. For $\lambda \gtrapprox 0.35$, the optimal PCS reduce to either PA or PS as mentioned earlier. For plotting we choose to set $r_a = r_b = 1$, so the curve of PCS overlaps exactly with that of PA for $\lambda \gtrapprox 0.35$.

It would a practical consideration to achieve better detecting performance with minimum signal strength. To get some insights, we plot entanglement per used photon $E/\langle n \rangle$ with respect to λ in

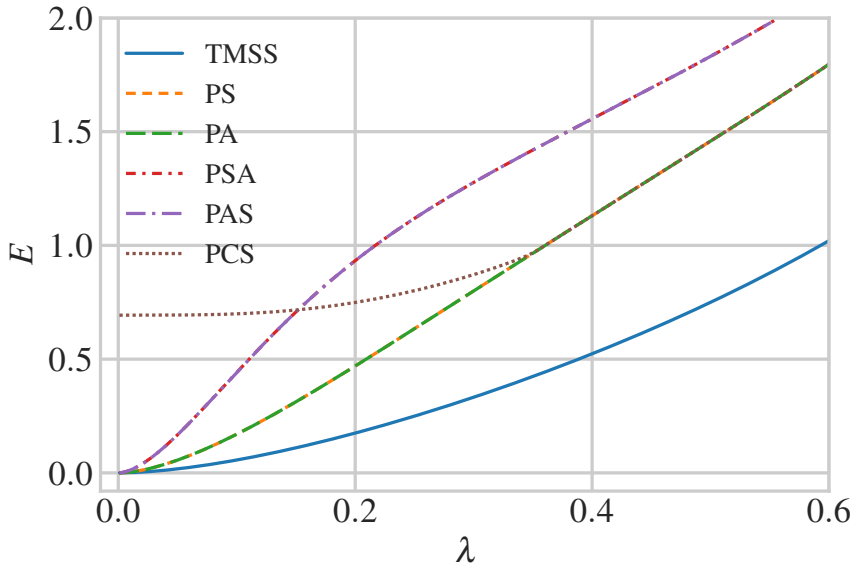

(a) Entanglement of E

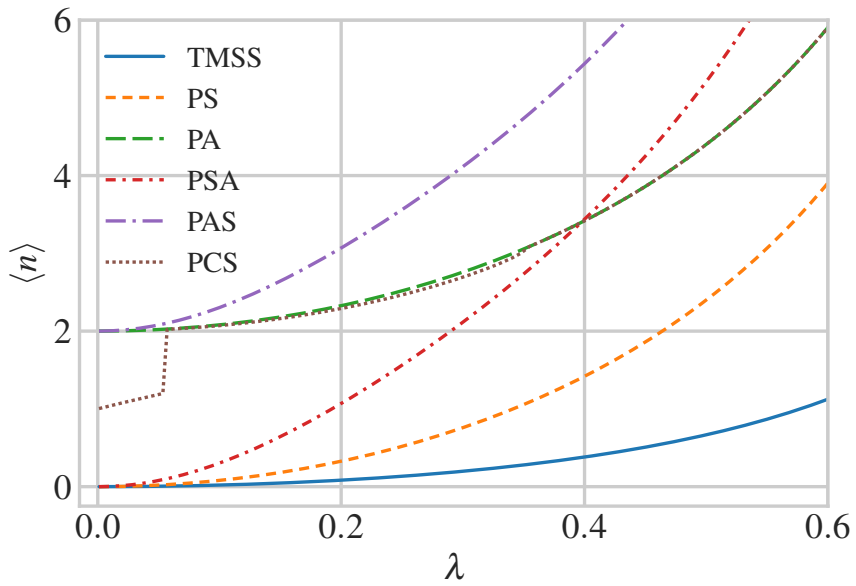

(b) Average photon numbers $\langle n \rangle$

Figure 4.2: Entropy of entanglement E and signal strength $\langle n \rangle$ for TMSS and non-Gaussian states under given values of λ ranging from 0.0 to 0.6. (a) Comparison of entanglement E among states with respect to λ. Here we have extra notes for PCS states. As a PCS state is determined by three variable r_a, r_b, and λ, its entanglement E still varies with respect to r_a and r_b when λ is given. In this figure, the curve of PCS states shows the maximum E can be obtained for each λ, i.e., the optimal pairs of r_a and r_b for each λ are used for plotting the curve of PCS states. (b) Comparison of average photon numbers $\langle n \rangle$ among states with respect to λ. The values of r_a and r_b used for PCS states for each given λ are the same with those used in Fig. 4.2a, i.e. the optimal ones result in the largest entanglement.

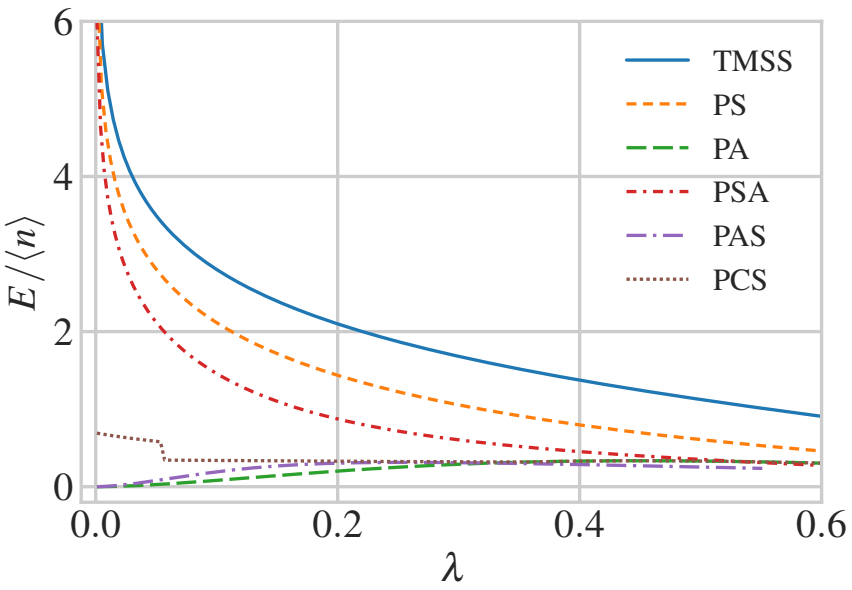

Figure 4.3: Comparison of $E/\langle n\rangle$ among states with respect to λ. The values of r_a and r_b used for PCS states for each given λ are the same with those used in Fig. 4.2a.

Fig. 4.3 for all these states. It is shown that TMSS is the most 'efficient' one to obtain entanglement with the least photon numbers. We could expect that TMSS would perform best for quantum illumination if we have constraints on signal strength.

PCS states are interesting as they have free choices on r_a and r_b. Four examples to show how entanglement depends on r_a and r_b are illustrated in Fig. 4.4. It is obvious that the mode A and B are equivalent so that the plots are symmetrical around the anti-diagonal. Numerical results show that for $\lambda \lessapprox 0.05$, the optimal choices are symmetrical states so that $r_a = r_b$. Then the optimal points move to the edge as λ increases, i.e., $r_a = 1$ or $r_b = 1$. Finally the optimal points stay on two anti-diagonal vertices.

4.2 Comparison of performance

Photon subtracted two-mode squeezed state (PS-TMSS) has been compared with TMSS for quantum illumination [82]. The comparison between these two kind of states was made under the same squeezing strength of detecting states. Here we extend the comparison to all non-Gaussian states we have mentioned in Eq. (4.6) and Eq. (4.8). We carry out numerical calculations of the

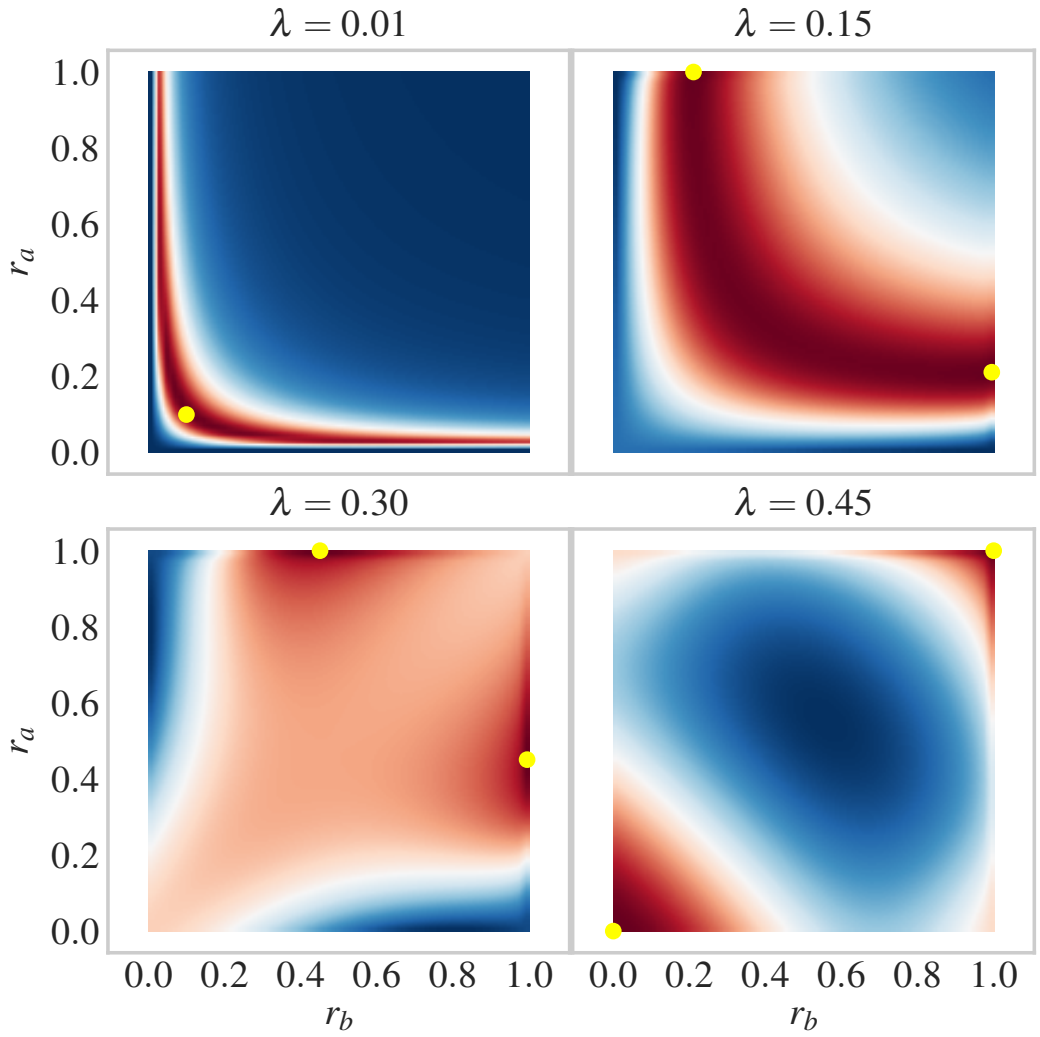

Figure 4.4: Entropy of entanglement with respect to r_a and r_b for PCS states under four different values of λ. All four sub-plots are symmetrical about $r_a = r_b$. Optimal points which have the largest entanglement have been labeled in each plot by solid yellow dots. They are: $(0.100, 0.100)$ for $\lambda = 0.01$, $(0.211, 1.00)$ and $(1.00, 0.211)$ for $\lambda = 0.15$, $(0.451, 1.00)$ and $(1.00, 0.451)$ for $\lambda = 0.30$, $(0.0, 0.0)$ and $(1.0, 1.0)$ for $\lambda = 0.45$.

quantum Chernoff bound and the Helstrom limit for $N = 1$ using Eq. (4.2) and Eq. (4.3) to evaluate the performance. We first make comparison of performance under the same squeezing strength in Sec. 4.2.1 as like what has been done in the Ref. [82]. Then, in Sec. 4.2.2 we make comparison under the signal strength of mode B.

Setup: As mentioned in Ref. [79, 80], quantum illumination shows its advantage under low signal-to-noise ratios. Also it has to mention that these two mode states approaches classical-state behavior when their signal strength is large enough [80]. Therefore, throughout our numerical calculations, we set up a scenario with low signal-to-noise ratios. The reflectance of suspect object $R = 0.01$. The average photon numbers of thermal noise has a relatively large value that $N_{\mathrm{th}} = 1.0$. Values of λ are also limited to be below 0.6 in order to keep the signal strength of detection states small enough. In such a scenario, error probability for detection using one copy of state is close to 0.5, as the signal is too weak to distinguish between two possible output states.

Methods: We use Python, NumPy, Scipy, and the QuTiP [108, 109] toolbox for numerical calculations. Matplotlib and Seaborn are used for plotting figures. First, we create all these two mode states shown in Eq. (4.5)(4.6)(4.8) by summation of tensor product of fock states over n from 0 to 31. For example in Python script, after "import numpy as np" and "import qutip as qu", we can create a TMSS by "tmss = qu.Qobj(numpy.sum([lambda ** n * qu.tensor(qu.basis(n_max, n), qu.basis(n_max, n)) for n in np.arange(n_max)])).unit()", where "n_max = 32" is the truncated photon number. All the states used for numerical calculation are normalized by ".unit()". The two mode mixing operator $U(\xi) = \exp\left(\xi a_B^\dagger a_C - \xi^* a_B a_C^\dagger\right)$ can be created by first creating a destroy operator "a = qu.destroy(n_max)" and then "U = s * qu.tensor(a.dag(), a) - np.conj(s) * qu.tensor(a, a.dag())". With these density matrix and operators created, we can obtain ρ_0 and ρ_1 shown in Eq. (4.1), and the Helstrom limit shown in Eq. (4.2). It can be done straightforwardly using methods of tensor product, partial trace, and trace norm, which are pre-defined in the QuTiP toolbox. The numerical calculation of quantum Chernoff bound takes some extra efforts as optimal t needs to be found. It is fulfilled by using the "minimize" method from "scipy.optimize".

4.2.1 Under the same squeezing strength

We first study how performance changes with respect to λ and then compare the performance of different states under the same λ. The results for quantum Chernoff bound and Helstrom limit are illustrated in Fig. 4.5a and Fig. 4.5b respectively. The two figures show similar results and conclusions. First we discuss the states except PCS. The rank of performance, from the top to the bottom, is in the order of PAS, PSA, PA, PS, and TMSS. The ranking order can be understood by looking into Fig. 4.2. For a given value of λ, PSA and PAS have the most enhanced entanglement, then PS and PA follow. TMSS has the smallest entropy of entanglement. Meanwhile PAS (PA) has larger signal strength than PSA (PS). As both the entanglement strength and the signal strength affect the performance, it explains why we get the ranking order mentioned above.

In Fig. 4.5, we plot two curves for PCS states, labeled by “PCS-etgl" and “PCS-opt" respectively. For the curve of “PCS-etgl", we choose those r_a and r_b which leads to the largest entanglement as like what we do in Fig. 4.2. Meanwhile the ‘PCS-opt’ curve is the lowest error probability a PCS state can achieve given a specific λ. In the region where λ is smaller than about 0.17, PCS outperforms all other states, which results from its advantage in both entanglement and signal strength as shown in Fig. 4.2. We find the similar stairs jumping at about the same positions ($\lambda \approx 0.05$) in both Fig. 4.5 and Fig. 4.2b, which indicates the signal strength has an impact on the performance.

The deviation between curves of “PCS-etgl" and “PCS-opt" also shows that entanglement is not the only factor determining the performance of quantum illumination. The choices of r_a and r_b which result in the largest entanglement do not always lead to the lowest quantum Chernoff bound, because the signal strength also matters. Here is an example for the case where $\lambda = 0.0995$ (such that $\langle n_B \rangle = 0.01$ for TMSS), $N_{th} = 1.0$, and $R = 0.01$. The optimal points which have the largest entanglement are A $(0.140, 1.0)$ and B $(1.0, 0.140)$. The corresponding quantum Chernoff bounds are 0.499124 and 0.499550 respectively. Meanwhile, the lowest quantum Chernoff bound can be achieved under the same λ is 0.499081, which is obtained at the point C $(0.118, 0.950)$. It is very close to point A, which has the maximum entanglement. Point C has entanglement of 0.688 and

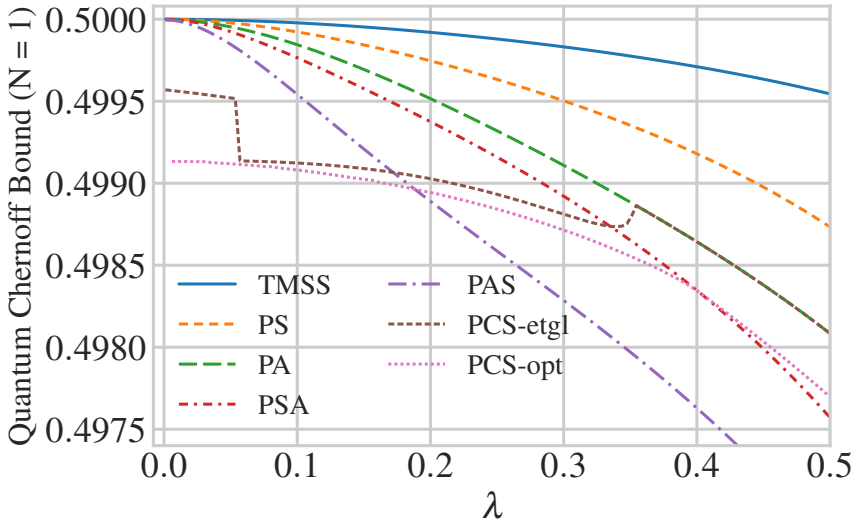

(a) Quantum Chernoff bounds with respect to λ for quantum illumiantion using a single copy of detecting state ($N = 1$). Here we set $N_{th} = 1.0$ and $R = 0.01$.

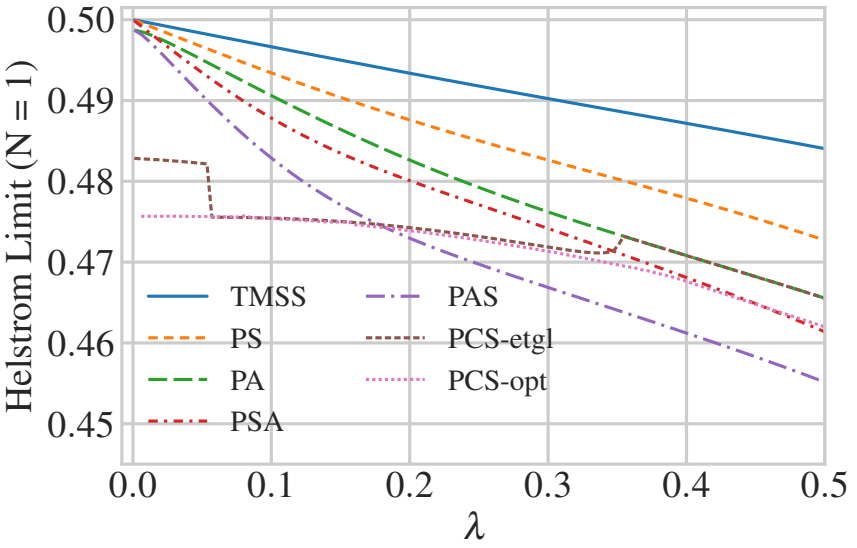

(b) Helstrom limits with respect to λ for quantum illumiantion using a single copy of detecting state ($N = 1$). Here we set $N_{th} = 1.0$ and $R = 0.01$.

Figure 4.5: (a) Quantum Chernoff bound and (b) Helstrom limit with respect to λ for quantum illumination using a single copy of detecting state ($N = 1$). Here we have some extra notes for PCS states. It shown that two curves for PCS states are plotted in both sub-plots (a) and (b). The points for the curve of “PCS-etgl" are constituted with PCS states which have the largest entanglement under a given λ, i.e., the r_a and r_b used here are the same with what we use for plotting Fig. 4.2a. Meanwhile, the curve of “PCS-opt" shows the optimal lowest quantum Chernoff bound which a PCS state can reach for each specific value of λ.

$\langle n_B \rangle$ of 1.544. Meanwhile point A has entanglement of 0.699 and $\langle n_B \rangle$ of 1.529. Even though the former one has less entanglement strength, it has larger signal strength. The overall effect makes point C achieve the lowest quantum Chernoff bound.

In summary, we could further improve the performance of quantum illumination by applying various non-Gaussian operations, as such operation can enhance the entanglement and the signal strength of the detecting states at the same time. Among all these non-Gaussian states, PCS performs the best under small squeezing strength, as it can enhance the entanglement by the most.

4.2.2 Under the same signal strength

From Fig. 4.2 we learn that non-Gaussian operations on TMSS will not only enhance entanglement, but also bring larger average photon numbers. Both factors can enhance the performance of quantum illumination. The former is quantum effect, while the latter is purely classical. Furthermore, in practice we would like to achieve the same performance with less power, particularly less power of the mode B. As a large detecting signal can also be detected by the other party we would like to detect, which exposes ourselves. As the mode B is sent out for detection, a constraint on its signal strength could be a practical consideration.

As entanglement is the key resource of quantum illumination, we first explore how the entropy of entanglement E varies with respect to different states under the same the signal strength of mode B. The results are shown in Fig. 4.6. We find that TMSS has the largest E than any other states under the same $\langle n_B \rangle$. PCS can has different values of E even for the same $\langle n_B \rangle$ because of the multiple choices of r_a and r_b, so we show points of PCS with scatter plot. An upper boundary of all possible PCS points is observed, which exactly overlap with the curve of PS. Therefore, given an arbitrary value of $\langle n_B \rangle$, the optimally chosen PCS states can only perform as best as PS states. No PCS state can achieves larger E than TMSS. The states constituting the “PCS-etgl" curve in Fig. 4.6 are the same with what we use in Fig. 4.2. It is far below the upper boundary. Since their r_a and r_b are optimized for each λ, they are no more the optimal choices for a given $\langle n_B \rangle$. Given the same $\langle n_B \rangle$, the optimal PCS which has the largest entanglement reduce to a PS state.

The above results for E vs. $\langle n_B \rangle$ give us some clue on the strategy of how to choose the optimal

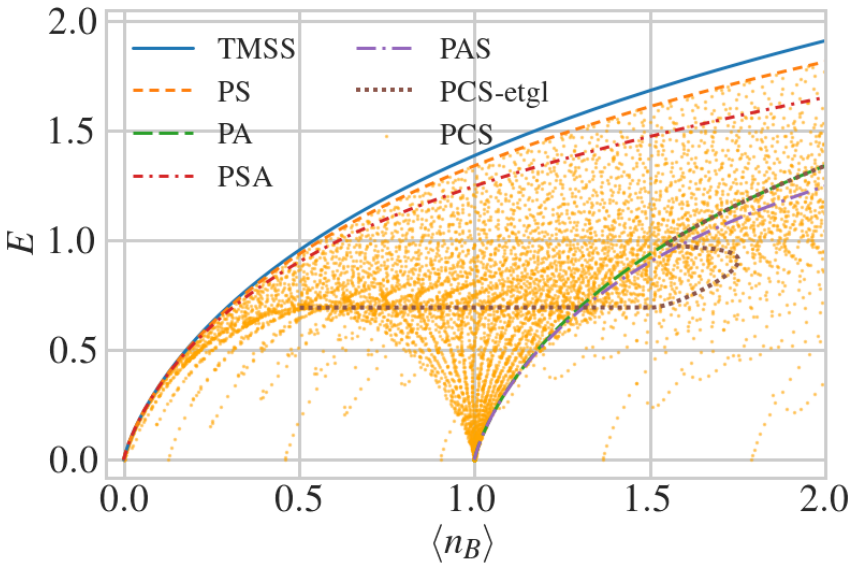

Figure 4.6: Entropy of entanglement vs. average photon number $\langle n_B \rangle$ of the mode B. r_a and r_b are sampled for PCS states, therefore we get scattered points. TMSS has the largest entropy of entanglement among these states when they all have the same $\langle n_B \rangle$. The points of PCS are bounded by the curve of PS from the top. (Notice that states used for plotting 'PCS-etlg' are optimized for each λ, they are no more the optimal states with the largest entanglement for each $\langle n_B \rangle$. For the same $\langle n_B \rangle$, PCS states can have different combinations of r_a, r_b, and λ, so we observe the u-turn shape of the 'PCS-etgl' curve around 1.6.)

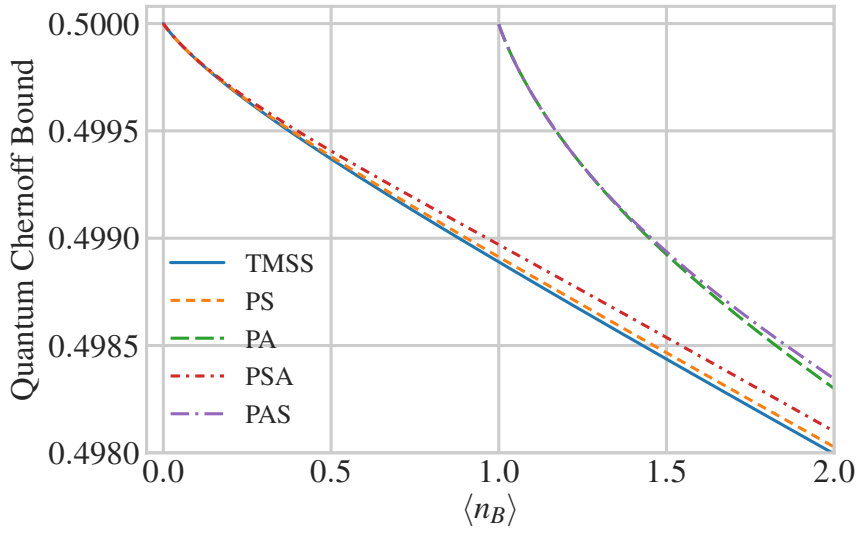

(a) In this figure, we compare Quantum Chernoff bounds among states excpet PCS under the same signal strenght, i.e., the same average photon number $\langle n_B \rangle$ of the mode B. It is shown that given the same $\langle n_B \rangle$, detecting using TMSS can get the lowest quantum Chernoff bound.

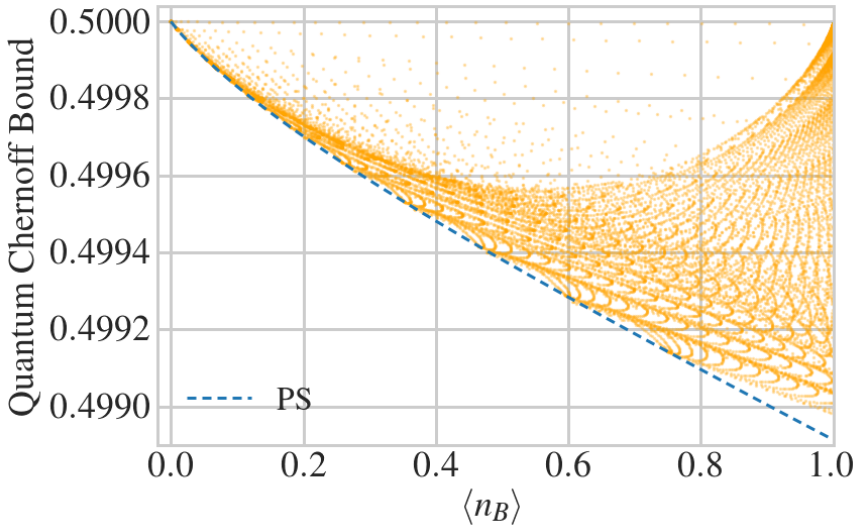

(b) Here we shown quantum Chernoff bounds of PCS states with respect to the signal strength of detecting states. Again we sample r_a and r_b to plot scattered points. It is shown that these scattered points of PCS states are bounded by the curve of PS state from the bottom.

Figure 4.7: Quantum Chernoff bound with respect to the signal strength, i.e., the average photon number $\langle n_B \rangle$ of the mode B. Recall that the mode B is sent out for detection

detecting state. We would choose TMSS, as it has the largest entanglement under the same $\langle n_B \rangle$. We illustrate in Fig. 4.7 how quantum Chernoff bound changes with respect to $\langle n_B \rangle$ to show that our strategy is correct. TMSS achieves the lowest quantum Chernoff bound among these states under the same $\langle n_B \rangle$. then PS and PSA follows. PA and PAS fall far behind, particularly for $\langle n_B \rangle < 1$. Their minimum $\langle n_B \rangle$ is 1.0, however, the curves of other states start form $(0.0, 0.5)$. In Fig. 4.7b, PCS states with different values of r_a and r_b are sampled and shown with scatter plot. It is clearly seen that these scatter points are bounded by the curve of PS as like what we have observed in Fig. 4.6. So under the same $\langle n_B \rangle$, the optimal PCS state which achieves the lowest quantum Chernoff bound reduce to a PS state. The results shown here is rather different from the results shown in Fig. 4.5, where comparisons are made under the same squeezing strength. We get reversed ranking order from that in Sec. 4.2.1.

So the strategy of choosing optimal states for detecting depends on what constraints we have on states. First if we can choose detecting states freely, TMSS is the optimal one. If these is a constraint on the signal strength of mode B, TMSS can achieve the lowest quantum Chernoff bound for a given value of $\langle n_B \rangle$ as shown in Fig. 4.7a. Meanwhile if there is no constraint on the signal strength of mode B, TMSS is still the one cost the least detecting power when the same quantum Chernoff bound is obtained. Second if only have limited TMSS sources available in our lab, we could consider applying additional non-Gaussian operations on TMSS to obtain better performance.

It is notices that Fig. 4.7a is like a mirroring of Fig. 4.6 about the x-axis. Meantime in Sec. 4.2.1, Fig. 4.5a is like a mirroring of Fig. 4.2a. Both Fig. 4.6 and Fig. 4.2a show how entanglement changes. It again indicates that entanglement is the key quantum resource behind quantum illumination. Form the curves of entanglement, we can predict how well states perform in quantum illumination.

4.3 Asymmetrical PCS states

We have mentioned in Sec. 4.2.1 that the PCS states which have the largest entanglement under the same λ do not always result in the best performance. Here we show with an example to explain

the reason behind. First, we notice that the model of quantum illumination shown in Fig. 4.1 is asymmetrical, because the signal mode B and the idler mode A go through rather different channels. Second, recall that the PCS states can have asymmetrical operations on the two modes respectively as

$$\mathrm{PCS} = \sqrt{N_3}\left(t_a\hat{a} + r_a\hat{a}^\dagger\right)\left(t_b\hat{b} + r_b\hat{b}^\dagger\right)|\mathrm{TMSS}\rangle \tag{4.10}$$

By setting unequal values for r_a and r_b, we get asymmetrical PCS states. One aspect of asymmetry is that two modes can have different average photon numbers. We show how the average photon numbers of two modes change with respect to r_a and r_b in Fig. 4.8, where we set $\lambda = 0.0995$. It is not strange that each mode achieve the largest average photon number if its coefficient $r_i (i = a, b)$ for the creation operator is 1.0. As the mode B is sent out for detection, it must be large enough to resist noise.

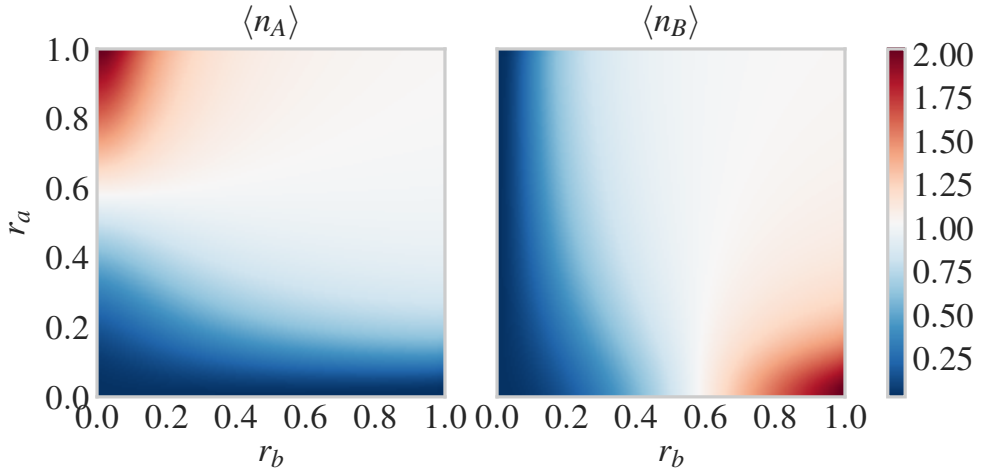

Figure 4.8: Average photon numbers of each mode for PCS states with respect to r_a and r_b. (left) Average photon numbers $\langle n_A\rangle$ of the mode A, which is retained in the lab. (right) Average photon numbers $\langle n_B\rangle$ of the mode B, which is sent out for detection. Here we set $\lambda = 0.0995$ in both the left and the right sub-plots. For comparison, TMSS with the same value of λ has an average photon number of 0.1 for each mode.

An example is illustrated in Fig. 4.9 to show how entanglement and signal strength affect the

performance of quantum illumination with PCS states. The parameters we set are $N_{\text{th}} = 1.0$, $R = 0.01$, and $\lambda = 0.0995$. The entropy of entanglement E is symmetrical with respect to the anti-diagonal, where $r_a = r_b$. There is a symmetrical L-shaped dark red band, where the state has larger entropy of entanglement. However, the quantum Chernoff bound is not symmetrical about the anti-diagonal. There is still a L-shaped band, which matches roughly the L-shaped band shown in the figure of E. However, the optimal area which has lower quantum Chernoff bound moves to the bottom right corner of the L-shaped band, where $\langle n_B \rangle$ is larger as shown in Fig. 4.8. The results for the quantum Chernoff bound are as expected, because both the entanglement and the signal strength affect the performance of quantum illumination. Therefore when we use PCS states for quantum illumination, an asymmetrical one where $\langle n_B \rangle > \langle n_A \rangle$ will outperform symmetrical input states where $\langle n_B \rangle = \langle n_A \rangle$.

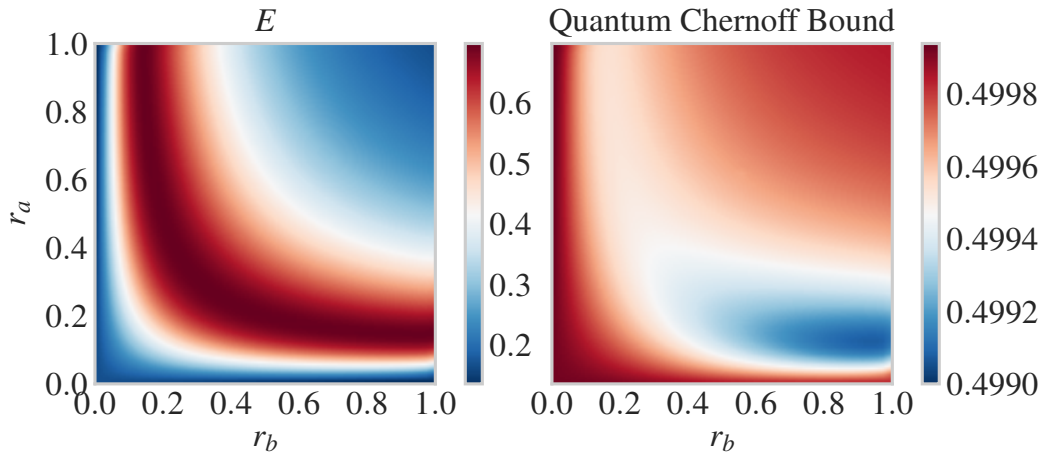

Figure 4.9: (left) Entropy of entanglement for PCS states with respect to r_a and r_b. (right) Quantum Chernoff bound for PCS states with respect to r_a and r_b. In both the right and the left sub-plots, we set $N_{\text{th}} = 1.0$, $R = 0.01$, and $\lambda = 0.0995$.

The results shown here again prove our conclusion that both the entanglement and the signal strength of the detecting state would affect the error probability of quantum illumination. From the quantum side of view, larger amount of entanglement results in larger quantum correlations

between two modes. From the classical side of view, stronger signals are less vulnerable to noisy and lossy environment.

5. SUMMARY AND CONCLUSIONS

We have studied the trade-off relation between information gain and output fidelity for the case of a QND measurement of photon numbers based on a cavity-QED setup. The information gain has been quantified either by I_M based on the mutual information or by I_F based on the concept of classical fidelity. In particular, we have investigated from an information theoretic viewpoint how the information gain and the output fidelity behave as we vary the measurement strength or the number N of successive measurements. We have shown that both the information quantifiers I_M and I_F exhibit very similar behaviors for all cases considered here (qubit states and coherent states), thus the trade-off relation between information gain and the output fidelity remains almost the same regardless of the measure of information gain.

To illustrate our analysis, we have considered two specific classes of initial states – qubit states and coherent states. In either case, the cavity is initially prepared in an unknown pure state with a certain probability. For a single weak measurement, the optimal measurement strength depends on the range of all possible photon numbers and a stronger measurement does not necessarily lead to more information gain. For the case of successive weak measurements, the information gain increases monotonically with respect to the number N of measurements, while the fidelity shows an oscillatory decreasing behavior. This results from the interference terms with different photon numbers. Thus, more information gain does not always lead to a worse fidelity. This may deserve further study to gain more insight into the trade-off relation occurring in quantum measurements, which may also have some practical implications.

When it comes to state protection using quantum measurement reversal, we first reviewed the ideal three-stage protection using monitored partial measurement and quantum reversal. We pointed out that it does not actually 'suppress' amplitude damping, but just selects and restores uncollapsed states and discards the others. So it is required that the monitoring efficiency, on which the selection relies on, should be perfectly 100%. Then we studied how quantum states evolve under three-stage protection with finite effective monitoring efficiency. Single-qubit states and

two-qubits entangled states were studied. Fidelity and concurrence were calculated to evaluate the performance. Theoretical expressions were derived, and specific numerical results were illustrated in plots. A criterion that decides whether to use the three-stage protection was given. The optimal strategy of applying the protocol was also studied.

Monitoring efficiency influences the effects of the three-stage protection a lot and should be considered carefully in practice. Introducing a monitored partial measurement of strength p_{s} at the first stage has dichotomy effects especially under finite monitoring efficiency. In one hand, it brings qubits closer to the ground state and makes them less vulnerable to amplitude damping. In the other hand, the monitored partial measurement itself is also a amplitude-damping process, therefore it introduces extra equivalent damping strength. Such negative effect becomes distinct under non-ideal monitoring. Generally the effect of the three-stage protection is weakened under finite monitoring efficiency. And the negative effect dominates when the original amplitude-damping strength d is weaker and p_{s} is strong. If the criterion for $\bar{\eta}$ given in Eq. (3.17) cannot be satisfied, it is better to seek other protection protocols for help. A detection-free monitoring protocol similar to what is demonstrated in the linear optical setup could be a good solution. However, its feasibility for other physical implementations still needs to be studied. A general detection-free protocol may be of interest for further research.

We also explored the performance of different two-mode entangled states for quantum illumination, including TMSS and non-Gaussian states obtained by applying photon subtraction and photon addition operations to TMSS. We evaluated the Helstrom limits and the quantum Chernoff bounds with respect to squeezing strength and signal strength. Then we compare the performance of these non-Gaussian states. We also explored the performance of asymmetrical PCS states generated by an asymmetrical coherent superposition of both photon subtraction and addition.

We conclude that non-Gaussian operations can enhance the performance of quantum illumination, i.e., obtain lower error probability, by introducing both larger entanglement and larger average photon numbers. Both factors affect the performance of quantum illumination, the former is a quantum effect, and the latter is a classical one. However, if the signal strength must

be constrained, TMSS performs the best given the same average photon number. When choosing PCS as the detecting state, we would consider an asymmetrical configurations to achieve lower error probability by making the signal (mode B) stronger than the idler (mode A). It is also possible to make many other kinds asymmetrical non-Gaussian states beside PCS stats. For example by two photon-subtraction operations on one mode and just one photon-addition on the other. The asymmetrical properties of the quantum illumination channel need further study to find the optimal detecting states.

REFERENCES

[1] M. A. Nielsen and I. L. Chuang, *Quantum computation and quantum information*. Cambridge University Press, 2010.

[2] H. M. Wiseman and G. J. Milburn, *Quantum measurement and control*. Cambridge University Press, 2009.

[3] M. M. Wilde, *Quantum Information Theory*. Cambridge University Press, 2013.

[4] K. Jacobs, *Quantum measurement theory and its applications*. Cambridge University Press, 2014.

[5] M. O. Scully and M. S. Zubairy, *Quantum Optics*. Cambridge University Press, 1997.

[6] P. Kok and B. W. Lovett, *Introduction to optical quantum information processing*. Cambridge University Press, 2010.

[7] von Neumann, *Mathematical Foundations of Quantum Mechanics*. Princeton University Press, Princeton, 1955.

[8] C. A. Fuchs and A. Peres, "Quantum-state disturbance versus information gain: Uncertainty relations for quantum information," *Phys. Rev. A*, vol. 53, pp. 2038–2045, Apr 1996.

[9] K. Banaszek, "Fidelity balance in quantum operations," *Phys. Rev. Lett.*, vol. 86, pp. 1366–1369, Feb 2001.

[10] L. Mišta Jr and R. Filip, "Quantum nondemolition measurement saturates fidelity trade-off," *Phys. Rev. A*, vol. 72, no. 3, p. 034307, 2005.

[11] M. F. Sacchi, "Information-disturbance tradeoff in estimating a maximally entangled state," *Phys. Rev. Lett.*, vol. 96, p. 220502, Jun 2006.

[12] L. Maccone, "Information-disturbance tradeoff in quantum measurements," *Phys. Rev. A*, vol. 73, p. 042307, Apr 2006.

[13] F. Sciarrino, M. Ricci, F. De Martini, R. Filip, and L. Mišta, "Realization of a minimal disturbance quantum measurement," *Phys. Rev. Lett.*, vol. 96, p. 020408, Jan 2006.

[14] F. Buscemi, M. Hayashi, and M. Horodecki, "Global information balance in quantum measurements," *Phys. Rev. Lett.*, vol. 100, p. 210504, May 2008.

[15] H. Terashima, "Information and fidelity in projective measurements," *Phys. Rev. A*, vol. 85, no. 2, p. 022124, 2012.

[16] H. Terashima, "Information, fidelity, and reversibility in single-qubit measurements," *Phys. Rev. A*, vol. 83, no. 3, p. 032114, 2011.

[17] Y. W. Cheong and S.-W. Lee, "Balance between information gain and reversibility in weak measurement," *Phys. Rev. Lett.*, vol. 109, no. 15, p. 150402, 2012.

[18] M. Ueda and M. Kitagawa, "Reversibility in quantum measurement processes," *Phys. Rev. Lett.*, vol. 68, pp. 3424–3427, Jun 1992.

[19] A. Imamoglu, "Logical reversibility in quantum-nondemolition measurements," *Phys. Rev. A*, vol. 47, pp. R4577–R4580, Jun 1993.

[20] A. Royer, "Reversible quantum measurements on a spin 1/2 and measuring the state of a single system," *Phys. Rev. Lett.*, vol. 73, pp. 913–917, Aug 1994.

[21] M. Ueda, N. Imoto, and H. Nagaoka, "Logical reversibility in quantum measurement: General theory and specific examples," *Phys. Rev. A*, vol. 53, pp. 3808–3817, Jun 1996.

[22] M. Ban, "Probabilistically reversible measurements," *Journal of Physics A: Mathematical and General*, vol. 34, no. 45, p. 9669, 2001.

[23] A. N. Korotkov and A. N. Jordan, "Undoing a weak quantum measurement of a solid-state qubit," *Phys. Rev. Lett.*, vol. 97, p. 166805, Oct 2006.

[24] N. Katz, M. Neeley, M. Ansmann, R. C. Bialczak, M. Hofheinz, E. Lucero, A. O'Connell, H. Wang, A. N. Cleland, J. M. Martinis, and A. N. Korotkov, "Reversal of the weak mea-

surement of a quantum state in a superconducting phase qubit," *Phys. Rev. Lett.*, vol. 101, p. 200401, Nov 2008.

[25] Y.-S. Kim, Y.-W. Cho, Y.-S. Ra, and Y.-H. Kim, "Reversing the weak quantummeasurement for a photonic qubit," *Opt. Express*, vol. 17, no. 14, pp. 11978–11985, 2009.

[26] Q. Sun, M. Al-Amri, and M. S. Zubairy, "Reversing the weak measurement of an arbitrary field with finite photon number," *Phys. Rev. A*, vol. 80, p. 033838, Sep 2009.

[27] P. W. Shor, "Scheme for reducing decoherence in quantum computer memory," *Phys. Rev. A*, vol. 52, pp. R2493–R2496, Oct 1995.

[28] A. M. Steane, "Error correcting codes in quantum theory," *Phys. Rev. Lett.*, vol. 77, no. 5, p. 793, 1996.

[29] M. Reed, L. DiCarlo, S. Nigg, L. Sun, L. Frunzio, S. Girvin, and R. Schoelkopf, "Realization of three-qubit quantum error correction with superconducting circuits," *Nature*, vol. 482, no. 7385, pp. 382–385, 2012.

[30] G. Waldherr, Y. Wang, S. Zaiser, M. Jamali, T. Schulte-Herbruggen, H. Abe, T. Ohshima, J. Isoya, J. F. Du, P. Neumann, and J. Wrachtrup, "Quantum error correction in a solid-state hybrid spin register," *Nature*, vol. 506, pp. 204–207, Feb 2014.

[31] B. M. Terhal, "Quantum error correction for quantum memories," *Rev. Mod. Phys.*, vol. 87, no. 2, p. 307, 2015.

[32] A. G. Fowler, M. Mariantoni, J. M. Martinis, and A. N. Cleland, "Surface codes: Towards practical large-scale quantum computation," *Phys. Rev. A*, vol. 86, no. 3, p. 32324, 2012.

[33] R. Barends, J. Kelly, A. Megrant, A. Veitia, D. Sank, E. Jeffrey, T. C. White, J. Mutus, A. G. Fowler, B. Campbell, Y. Chen, Z. Chen, B. Chiaro, A. Dunsworth, C. Neill, P. O'Malley, P. Roushan, A. Vainsencher, J. Wenner, A. N. Korotkov, A. N. Cleland, and J. M. Martinis, "Superconducting quantum circuits at the surface code threshold for fault tolerance," *Nature*, vol. 508, pp. 500–503, Apr 2014.

[34] A. Y. Kitaev, "Fault-tolerant quantum computation by anyons," *Annals of Physics*, vol. 303, no. 1, pp. 2–30, 2003.

[35] C. Nayak, S. H. Simon, A. Stern, M. Freedman, and S. Das Sarma, "Non-abelian anyons and topological quantum computation," *Rev. Mod. Phys.*, vol. 80, pp. 1083–1159, Sep 2008.

[36] J. D. Sau, R. M. Lutchyn, S. Tewari, and S. D. Sarma, "Generic new platform for topological quantum computation using semiconductor heterostructures," *Phys. Rev. Lett.*, vol. 104, no. 4, p. 040502, 2010.

[37] J. Alicea, Y. Oreg, G. Refael, F. von Oppen, and M. P. A. Fisher, "Non-Abelian statistics and topological quantum information processing in 1D wire networks," *Nat. Phys.*, vol. 7, no. 5, pp. 412–417, 2011.

[38] P. Zanardi and M. Rasetti, "Noiseless quantum codes," *Phys. Rev. Lett.*, vol. 79, no. 17, p. 3306, 1997.

[39] D. A. Lidar, I. L. Chuang, and K. B. Whaley, "Decoherence-free subspaces for quantum computation," *Phys. Rev. Lett.*, vol. 81, no. 12, p. 2594, 1998.

[40] P. G. Kwiat, A. J. Berglund, J. B. Altepeter, and A. G. White, "Experimental verification of decoherence-free subspaces," *Science*, vol. 290, no. 5491, pp. 498–501, 2000.

[41] L. Viola and S. Lloyd, "Dynamical suppression of decoherence in two-state quantum systems," *Phys. Rev. A*, vol. 58, pp. 2733–2744, Oct 1998.

[42] L. Viola, E. Knill, and S. Lloyd, "Dynamical decoupling of open quantum systems," *Phys. Rev. Lett.*, vol. 82, no. 12, p. 2417, 1999.

[43] M. J. Biercuk, H. Uys, A. P. VanDevender, N. Shiga, W. M. Itano, and J. J. Bollinger, "Optimized dynamical decoupling in a model quantum memory," *Nature*, vol. 458, pp. 996–1000, Apr 2009.

[44] G. De Lange, Z. Wang, D. Riste, V. Dobrovitski, and R. Hanson, "Universal dynamical decoupling of a single solid-state spin from a spin bath," *Science*, vol. 330, no. 6000, pp. 60–63, 2010.

[45] T. van der Sar, Z. H. Wang, M. S. Blok, H. Bernien, T. H. Taminiau, D. M. Toyli, D. A. Lidar, D. D. Awschalom, R. Hanson, and V. V. Dobrovitski, "Decoherence-protected quantum gates for a hybrid solid-state spin register," *Nature*, vol. 484, pp. 82–86, Apr 2012.

[46] A. Royer, "Reversible quantum measurements on a spin and measuring the state of a single system," *Phys. Rev. Lett.*, vol. 74, pp. 1040–1040, Feb 1995.

[47] H. Mabuchi and P. Zoller, "Inversion of quantum jumps in quantum optical systems under continuous observation," *Phys. Rev. Lett.*, vol. 76, no. 17, p. 3108, 1996.

[48] M. A. Nielsen and C. M. Caves, "Reversible quantum operations and their application to teleportation," *Phys. Rev. A*, vol. 55, pp. 2547–2556, Apr 1997.

[49] M. Koashi and M. Ueda, "Reversing measurement and probabilistic quantum error correction," *Phys. Rev. Lett.*, vol. 82, no. 12, p. 2598, 1999.

[50] A. N. Korotkov and A. N. Jordan, "Undoing a weak quantum measurement of a solid-state qubit," *Phys. Rev. Lett.*, vol. 97, no. 16, p. 166805, 2006.

[51] N. Katz, M. Neeley, M. Ansmann, R. C. Bialczak, M. Hofheinz, E. Lucero, A. O'Connell, H. Wang, A. N. Cleland, J. M. Martinis, and A. N. Korotkov, "Reversal of the weak measurement of a quantum state in a superconducting phase qubit," *Phys. Rev. Lett.*, vol. 101, p. 200401, Nov 2008.

[52] Q. Sun, M. Al-Amri, and M. S. Zubairy, "Reversing the weak measurement of an arbitrary field with finite photon number," *Phys. Rev. A*, vol. 80, no. 3, p. 033838, 2009.

[53] Y.-S. Kim, Y.-W. Cho, Y.-S. Ra, and Y.-H. Kim, "Reversing the weak quantum measurement for a photonic qubit," *Opt. Express*, vol. 17, no. 14, pp. 11978–11985, 2009.

[54] Q. Sun, M. Al-Amri, L. Davidovich, and M. S. Zubairy, "Reversing entanglement change by a weak measurement," *Phys. Rev. A*, vol. 82, p. 052323, Nov 2010.

[55] M. Al Amri, M. O. Scully, and M. S. Zubairy, "Reversing the weak measurement on a qubit," *J. Phys. B*, vol. 44, no. 16, p. 165509, 2011.

[56] Z. Liao, M. Al-Amri, and M. S. Zubairy, "Protecting quantum entanglement from amplitude damping," *J. Phys. B*, vol. 46, no. 14, p. 145501, 2013.

[57] X. Zeng, M. Al-Amri, S. Zhu, and M. S. Zubairy, "Proposal for reversing the weak measurement with arbitrary maximum photon number," *Phys. Rev. A*, vol. 93, p. 53826, May 2016.

[58] S. S. Esfahani, Z. Liao, and M. S. Zubairy, "Robust quantum state recovery from amplitude damping within a mixed states framework," *J. Phys. B At. Mol. Opt. Phys.*, vol. 49, no. 15, p. 155501, 2016.

[59] A. N. Korotkov and K. Keane, "Decoherence suppression by quantum measurement reversal," *Phys. Rev. A*, vol. 81, no. 4, p. 040103, 2010.

[60] N. Katz, M. Ansmann, R. C. Bialczak, E. Lucero, R. McDermott, M. Neeley, M. Steffen, E. M. Weig, A. N. Cleland, J. M. Martinis, *et al.*, "Coherent state evolution in a superconducting qubit from partial-collapse measurement," *Science*, vol. 312, no. 5779, pp. 1498–1500, 2006.

[61] J.-C. Lee, Y.-C. Jeong, Y.-S. Kim, and Y.-H. Kim, "Experimental demonstration of decoherence suppression via quantum measurement reversal," *Opt. Express*, vol. 19, no. 17, pp. 16309–16316, 2011.

[62] Y.-S. Kim, J.-C. Lee, O. Kwon, and Y.-H. Kim, "Protecting entanglement from decoherence using weak measurement and quantum measurement reversal," *Nature Phys.*, vol. 8, no. 2, pp. 117–120, 2012.

[63] H.-T. Lim, J.-C. Lee, K.-H. Hong, and Y.-H. Kim, "Avoiding entanglement sudden death using single-qubit quantum measurement reversal," *Opt. Express*, vol. 22, no. 16, pp. 19055–19068, 2014.

[64] J.-C. Lee, H.-T. Lim, K.-H. Hong, Y.-C. Jeong, M. S. Kim, and Y.-H. Kim, "Experimental demonstration of delayed-choice decoherence suppression," *Nat. Commun.*, vol. 5, p. 4522, Jul 2014.

[65] Y. Zhong, Z. Wang, J. Martinis, A. Cleland, A. Korotkov, and H. Wang, "Reducing the impact of intrinsic dissipation in a superconducting circuit by quantum error detection," *Nat. Commun*, vol. 5, 2014.

[66] Z.-X. Man, Y.-J. Xia, and N. B. An, "Manipulating entanglement of two qubits in a common environment by means of weak measurements and quantum measurement reversals," *Phys. Rev. A*, vol. 86, p. 12325, Jul 2012.

[67] Z.-X. Man, Y.-J. Xia, and N. B. An, "Enhancing entanglement of two qubits undergoing independent decoherences by local pre- and postmeasurements," *Phys. Rev. A*, vol. 86, p. 52322, Nov 2012.

[68] C. Yao, Z.-H. Ma, Z.-H. Chen, and A. Serafini, "Robust tripartite-to-bipartite entanglement localization by weak measurements and reversal," *Phys. Rev. A*, vol. 86, p. 22312, Aug 2012.

[69] Z. He, C. Yao, and J. Zou, "Robust state transfer in the quantum spin channel via weak measurement and quantum measurement reversal," *Phys. Rev. A*, vol. 88, p. 44304, Oct 2013.

[70] X.-L. Zong, C.-Q. Du, M. Yang, Q. Yang, and Z.-L. Cao, "Protecting remote bipartite entanglement against amplitude damping by local unitary operations," *Phys. Rev. A*, vol. 90, no. 6, p. 062345, 2014.

[71] K. Xu, X. Y. LinPeng, and Z. L. Wang, "Decoherence suppression combining quantum uncollapsing and dynamical decoupling," *Appl. Phys. Lett.*, vol. 104, no. 26, p. 263509, 2014.

[72] S.-C. Wang, Z.-W. Yu, W.-J. Zou, and X.-B. Wang, "Protecting quantum states from decoherence of finite temperature using weak measurement," *Phys. Rev. A*, vol. 89, no. 2, p. 022318, 2014.

[73] J. He and L. Ye, "Protecting entanglement under depolarizing noise environment by using weak measurements," *Physica A*, vol. 419, pp. 7–13, 2015.

[74] B. Vlastakis, A. Petrenko, N. Ofek, L. Sun, Z. Leghtas, K. Sliwa, Y. Liu, M. Hatridge, J. Blumoff, L. Frunzio, M. Mirrahimi, L. Jiang, M. H. Devoret, and R. J. Schoelkopf, "Characterizing entanglement of an artificial atom and a cavity cat state with Bell/'s inequality," *Nat. Commun*, vol. 6, Nov 2015.

[75] F. Dell'Anno, S. De Siena, L. Albano, and F. Illuminati, "Continuous-variable quantum teleportation with non-gaussian resources," *Physical Review A*, vol. 76, no. 2, p. 022301, 2007.

[76] A. Ourjoumtsev, A. Dantan, R. Tualle-Brouri, and P. Grangier, "Increasing entanglement between gaussian states by coherent photon subtraction," *Physical Review Letters*, vol. 98, no. 3, p. 030502, 2007.

[77] Y. Yang and F.-L. Li, "Entanglement properties of non-gaussian resources generated via photon subtraction and addition and continuous-variable quantum-teleportation improvement," *Physical Review A*, vol. 80, no. 2, p. 022315, 2009.

[78] H.-J. Kim, J. Kim, and H. Nha, "Enhanced multipartite quantum correlation by non-gaussian operations," *Physical Review A*, vol. 88, no. 3, p. 032109, 2013.

[79] S. Lloyd, "Enhanced sensitivity of photodetection via quantum illumination," *Science*, vol. 321, no. 5895, pp. 1463–1465, 2008.

[80] S.-H. Tan, B. I. Erkmen, V. Giovannetti, S. Guha, S. Lloyd, L. Maccone, S. Pirandola, and J. H. Shapiro, "Quantum illumination with gaussian states," *Physical Review Letters*, vol. 101, no. 25, p. 253601, 2008.

[81] J. H. Shapiro and S. Lloyd, "Quantum illumination versus coherent-state target detection," *New Journal of Physics*, vol. 11, no. 6, p. 063045, 2009.

[82] S. Zhang, J. Guo, W. Bao, J. Shi, C. Jin, X. Zou, and G. Guo, "Quantum illumination with photon-subtracted continuous-variable entanglement," *Physical Review A*, vol. 89, no. 6, p. 062309, 2014.

[83] S.-Y. Lee and H. Nha, "Quantum state engineering by a coherent superposition of photon subtraction and addition," *Physical Review A*, vol. 82, no. 5, p. 053812, 2010.

[84] S.-Y. Lee, S.-W. Ji, H.-J. Kim, and H. Nha, "Enhancing quantum entanglement for continuous variables by a coherent superposition of photon subtraction and addition," *Physical Review A*, vol. 84, no. 1, p. 012302, 2011.

[85] H. Ollivier and W. H. Zurek, "Quantum discord: a measure of the quantumness of correlations," *Physical review letters*, vol. 88, no. 1, p. 017901, 2001.

[86] L. Henderson and V. Vedral, "Classical, quantum and total correlations," *Journal of physics A: mathematical and general*, vol. 34, no. 35, p. 6899, 2001.

[87] S. Ragy, I. R. Berchera, I. P. Degiovanni, S. Olivares, M. G. Paris, G. Adesso, and M. Genovese, "Quantifying the source of enhancement in experimental continuous variable quantum illumination," *JOSA B*, vol. 31, no. 9, pp. 2045–2050, 2014.

[88] C. Weedbrook, S. Pirandola, J. Thompson, V. Vedral, and M. Gu, "How discord underlies the noise resilience of quantum illumination," *New Journal of Physics*, vol. 18, no. 4, p. 043027, 2016.

[89] M. Bradshaw, S. M. Assad, J. Y. Haw, S.-H. Tan, P. K. Lam, and M. Gu, "Overarching framework between gaussian quantum discord and gaussian quantum illumination," *Phys. Rev. A*, vol. 95, p. 022333, Feb 2017.

[90] M. Brune, S. Haroche, V. Lefevre, J. M. Raimond, and N. Zagury, "Quantum nondemolition measurement of small photon numbers by rydberg-atom phase-sensitive detection," *Phys. Rev. Lett.*, vol. 65, no. 8, pp. 976–979, 1990.

[91] M. Brune, S. Haroche, J. M. Raimond, L. Davidovich, and N. Zagury, "Manipulation of photons in a cavity by dispersive atom-field coupling: Quantum-nondemolition measurements and generation of "schrödinger cat" states," *Phys. Rev. A*, vol. 45, no. 7, pp. 5193–5214, 1992.

[92] N. F. Ramsey, "A molecular beam resonance method with separated oscillating fields," *Phys. Rev.*, vol. 78, no. 6, pp. 695–699, 1950.

[93] C. E. Shannon, "A mathematical theory of communication," *Bell Syst. Tech. J.*, vol. 27, pp. 379–423, 623–656, 1948.

[94] D. V. Lindley, "On a measure of the information provided by an experiment," *Ann. Math. Statist.*, vol. 27, pp. 986–1005, 1956.

[95] C. A. Fuchs, "Distinguishability and accessible information in quantum theory," *arXiv preprint quant-ph/9601020*, 1996.

[96] V. Weisskopf and E. Wigner, "Berechnung der natürlichen linienbreite auf grund der diracschen lichttheorie," *Zeitschrift für Physik*, vol. 63, no. 1-2, pp. 54–73, 1930.

[97] A. Salles, F. de Melo, M. P. Almeida, M. Hor-Meyll, S. P. Walborn, P. H. Souto Ribeiro, and L. Davidovich, "Experimental investigation of the dynamics of entanglement: Sudden death, complementarity, and continuous monitoring of the environment," *Phys. Rev. A*, vol. 78, no. 2, p. 022322, 2008.

[98] W. K. Wootters, "Entanglement of formation of an arbitrary state of two qubits," *Phys. Rev. Lett.*, vol. 80, pp. 2245–2248, Mar 1998.

[99] R. Tahira, M. Ikram, S. Bougouffa, and M. S. Zubairy, "Entanglement dynamics of high-dimensional bipartite field states inside the cavities in dissipative environments," *J. Phys. B*, vol. 43, no. 3, p. 035502, 2010.

[100] C. W. Helstrom, "Quantum detection and estimation theory," *Journal of Statistical Physics*, vol. 1, no. 2, pp. 231–252, 1969.

[101] K. M. Audenaert, J. Calsamiglia, R. Muñoz-Tapia, E. Bagan, L. Masanes, A. Acin, and F. Verstraete, "Discriminating states: The quantum chernoff bound," *Physical Review Letters*, vol. 98, no. 16, p. 160501, 2007.

[102] S. L. Braunstein and P. Van Loock, "Quantum information with continuous variables," *Reviews of Modern Physics*, vol. 77, no. 2, p. 513, 2005.

[103] C. Weedbrook, S. Pirandola, R. García-Patrón, N. J. Cerf, T. C. Ralph, J. H. Shapiro, and S. Lloyd, "Gaussian quantum information," *Reviews of Modern Physics*, vol. 84, no. 2, p. 621, 2012.

[104] S. Guha and B. I. Erkmen, "Gaussian-state quantum-illumination receivers for target detection," *Physical Review A*, vol. 80, no. 5, p. 052310, 2009.

[105] E. Lopaeva, I. R. Berchera, I. Degiovanni, S. Olivares, G. Brida, and M. Genovese, "Experimental realization of quantum illumination," *Physical Review Letters*, vol. 110, no. 15, p. 153603, 2013.

[106] Z. Zhang, S. Mouradian, F. N. Wong, and J. H. Shapiro, "Entanglement-enhanced sensing in a lossy and noisy environment," *Physical Review Letters*, vol. 114, no. 11, p. 110506, 2015.

[107] Q. Zhuang, Z. Zhang, and J. H. Shapiro, "Optimum mixed-state discrimination for noisy entanglement-enhanced sensing," *Physical Review Letters*, vol. 118, no. 4, p. 040801, 2017.

[108] J. Johansson, P. Nation, and F. Nori, "Qutip: An open-source python framework for the dynamics of open quantum systems," *Computer Physics Communications*, vol. 183, no. 8, pp. 1760–1772, 2012.

[109] J. Johansson, P. Nation, and F. Nori, "Qutip 2: A python framework for the dynamics of open quantum systems," *Computer Physics Communications*, vol. 184, pp. 1234–1240, 2013.

[110] S. M. Barnett and S. Croke, "Quantum state discrimination," *Advances in Optics and Photonics*, vol. 1, no. 2, pp. 238–278, 2009.

[111] A. Chefles, "Quantum state discrimination," *Contemporary Physics*, vol. 41, no. 6, pp. 401–424, 2000.

APPENDIX A

EFFECTIVE DISPERSIVE ATOM-FIELD INTERACTION IN THE QND MEASUREMENT

Consider a three-level atomic system in a cascade configuration [90, 5]. The transitions $|i\rangle \rightarrow |e\rangle$ and $|e\rangle \rightarrow |f\rangle$ are allowed, and the transition $|i\rangle \rightarrow |f\rangle$ is forbidden. The frequency of cavity field ω is detuned from ω_{ie} by an amount $\Delta = \mu - \omega_{ie}$. Δ is small compared with other transitions. $|i\rangle$ and $|e\rangle$ are affected by the atom-field coupling, meanwhile $|f\rangle$ is not affected. Neglecting the

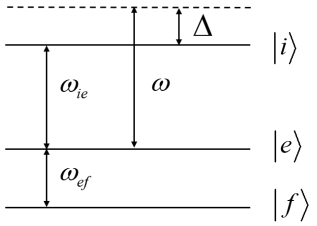

Figure A.1: Atomic Levels

far detuned level $|f\rangle$, we find the Hamiltonian for the atom-field interaction is given by

$$H = \frac{1}{2}\hbar\omega_{ie}\sigma_z + \hbar\omega aa^\dagger + \hbar g\left(\sigma_+ a + a^\dagger\sigma_-\right), \tag{A.1}$$

where $\sigma_z = |i\rangle\langle i| - |e\rangle\langle e|$, $\sigma_+ = |i\rangle\langle e|$, and $\sigma_- = |e\rangle\langle i|$. The Hamiltonian matrix in the basis of dressed states $|i, n-1\rangle \rightarrow |e, n\rangle$ is given by

$$H_n = \hbar\begin{bmatrix} (n-1)\omega + \frac{\omega_{ie}}{2} & g\sqrt{n} \\ g\sqrt{n} & n\omega - \frac{\omega_{ie}}{2} \end{bmatrix} \tag{A.2}$$

The eigen equation is $H_n |\psi_n\rangle = E_n |\psi_n\rangle$. The eigen values can be obtained by solving

$$\det \begin{bmatrix} (n-1)\omega + \frac{\omega_{ie}}{2} - \frac{E_n}{\hbar} & g\sqrt{n} \\ g\sqrt{n} & n\omega - \frac{\omega_{ie}}{2} - \frac{E_n}{\hbar} \end{bmatrix} = 0, \tag{A.3}$$

which turns to be

$$\frac{E_n^2}{\hbar^2} - (2n-1)\omega\frac{E_n}{\hbar} + \frac{1}{4}(2n-1)^2\omega^2 - \frac{\Delta^2}{4} - g^2 n = 0. \tag{A.4}$$

The solutions are

$$E_{n\pm} = \hbar\left(n - \frac{1}{2}\right)\omega \pm \frac{1}{2}\Omega_n, \tag{A.5}$$

where $\Omega_n = \sqrt{\Delta^2 + 4g^2 n}$. The corresponding eigenstates are

$$\begin{aligned} |\psi_{n+}\rangle &= \cos\frac{\phi}{2}|i, n-1\rangle + \sin\frac{\phi}{2}|e, n\rangle, \\ |\psi_{n-}\rangle &= -\sin\frac{\phi}{2}|i, n-1\rangle + \cos\frac{\phi}{2}|e, n\rangle, \end{aligned} \tag{A.6}$$

where

$$\phi = \arctan\left(-\frac{2g\sqrt{n}}{\Delta}\right), \quad \sin\frac{\phi}{2} = \sqrt{\frac{\Omega_n + \Delta}{2\Omega_n}}, \quad \text{and} \quad \cos\frac{\phi}{2} = \sqrt{\frac{\Omega_n - \Delta}{2\Omega_n}}. \tag{A.7}$$

Now we consider the case where Δ is large compared with $2g\sqrt{n}$, so that

$$\frac{2g\sqrt{n}}{\Delta} \ll 1, \quad \phi \to \pi_-, \quad \sin\frac{\phi}{2} \approx 1, \quad \cos\frac{\phi}{2} \approx 0, \quad \text{and} \quad \Omega_n \approx \Delta + \frac{2g^2 n}{\Delta} \tag{A.8}$$

Therefore the eigenstates and corresponding eigenvalues become

$$\begin{aligned} |\psi_{n+}\rangle &= |e, n\rangle, \quad E_{n+} = \hbar\left(n\omega - \frac{1}{2}\omega_{ie}\right) + \frac{\hbar g^2 n}{\Delta} \\ |\psi_{n-}\rangle &= |i, n-1\rangle, \quad E_{n-} = \hbar\left[(n-1)\omega + \frac{1}{2}\omega_{ie}\right] - \frac{\hbar g^2 n}{\Delta} \end{aligned} \tag{A.9}$$

We find that photon numbers are not changed, except that the energy levels are perturbed by either positive and negative $\frac{\hbar g^2 n}{\Delta}$ for $|e,n\rangle$ and $|i,n-1\rangle$. The energy shift per photon for $|e,n\rangle$ is

$$\delta = \frac{\hbar g^2}{\Delta}. \tag{A.10}$$

Therefor there is a coupling between cavity photon numbers and atomic level $|e\rangle$, whose strength is measured by δ. We can write the interaction Hamiltonian as

$$H_I = \frac{\hbar g^2}{\Delta} a^\dagger a \otimes |e\rangle\langle e| \,. \tag{A.11}$$

If we consider the atomic Hilbert space spanned by $|e\rangle$ and $|f\rangle$. The state $|f\rangle$ is not affected by the coupling. Therefore we have the effective Hamiltonian given by

$$H = \frac{\hbar}{2}\omega_{ef}\sigma_z + \hbar\omega a^\dagger a + \frac{\hbar g^2}{\Delta} a^\dagger a \sigma_+ \sigma_-, \tag{A.12}$$

where $\sigma_z = |e\rangle\langle e| - |f\rangle\langle f|$, $\sigma_+ = |e\rangle\langle f|$, and $\sigma_- = |f\rangle\langle e|$.

APPENDIX B

HELSTROM LIMIT AND QUANTUM CHERNOFF BOUND

B.1 Quantum state discrimination

Let us assume that a given quantum states is secretly prepared either in state ρ_0 or ρ_1 with probabilities π_0 and π_1 respectively. An observer's task is to perform any possible quantum measurement to make the "best" guess on the state's true identity. If the"best" here means the minimum error probability, we should find a proper set of $\{E_b\}$ to minimize

$$P_e \equiv \min_{\{\hat{E}_b\}} \sum_b \min \left\{ \pi_0 \mathrm{tr}(\hat{\rho}_0 \hat{E}_b),\, \pi_1 \mathrm{tr}(\hat{\rho}_1 \hat{E}_b) \right\}. \tag{B.1}$$

If we make a binary-valued POVM $\{E_0,\, E_1\}$ on the state, we get the minimum error probability as [110]

$$P_e = \pi_0 \,\mathrm{tr}(\hat{\rho}_0 \hat{E}_1) \,+\, \pi_1 \,\mathrm{tr}(\hat{\rho}_1 \hat{E}_0). \tag{B.2}$$

B.2 Helstrom limit

The optimal error probability to distinguish two quantum states is given by the Helstrom limit [111],

$$P_e = \frac{1}{2}\left(1 - \mathrm{tr}|\pi_1\rho_1 - \pi_0\rho_0|\right) = \frac{1}{2}\left(1 - \|\pi_1\rho_1 - \pi_0\rho_0\|_1\right), \tag{B.3}$$

where $|A| = \left(A^\dagger A\right)^{\frac{1}{2}}$, i.e. the norm of A. It can be proved as follows. First we introduce a Hermitian operator

$$\Gamma \equiv \pi_1\rho_1 - \pi_0\rho_0 = \sum_{k=1}^{d} \lambda_k \,|k\rangle\langle k| \tag{B.4}$$

Using the fact that $E_0 + E_1 = I$, we get

$$\begin{aligned} P_e &= \pi_0 \mathrm{tr}\Big(\hat{\rho}_0(I - \hat{E}_0)\Big) + \pi_1 \mathrm{tr}(\hat{\rho}_1 \hat{E}_0) \\ &= \pi_0 \mathrm{tr}\hat{\rho}_0 - \pi_0 \mathrm{tr}(\hat{\rho}_0 \hat{E}_0) + \pi_1 \mathrm{tr}(\hat{\rho}_1 \hat{E}_0) \\ &= \pi_0 + \mathrm{tr}\Big((\pi_1 \hat{\rho}_1 - \pi_0 \hat{\rho}_0)\hat{E}_0\Big) \\ &= \pi_0 + \mathrm{tr}\Big(\Gamma E_0\Big) = \pi_1 - \mathrm{tr}\Big(\Gamma E_1\Big). \end{aligned} \tag{B.5}$$

Using the spectral decomposition of Γ, we have

$$P_e = \pi_0 + \sum_k^d \lambda_k \langle k|E_0|k\rangle = \pi_1 - \sum_k^d \lambda_k \langle k|E_1|k\rangle \tag{B.6}$$

To make P_e as small as possible, we would like such a condition that $\sum_k^d \lambda_k \langle k|E_0|k\rangle$ is as small as possible and that $\sum_k^d \lambda_k \langle k|E_1|k\rangle$ is as large as possible. Γ is neither positive- nor negative-definite, suppose that

$$\begin{aligned} &\lambda_k < 0 \quad \text{for} \quad 1 \leq \mathrm{k} < \mathrm{k}_0 \\ &\lambda_k = 0 \quad \text{for} \quad \mathrm{k}_0 \leq \mathrm{k} < \mathrm{k}_1 \\ &\lambda_k > 0 \quad \text{for} \quad \mathrm{k}_1 \leq \mathrm{k} \leq \mathrm{d}. \end{aligned} \tag{B.7}$$

To satisfy the optimal condition mentioned above, the optimal measurement operators can be constructed as follows

$$E_0 = \sum_{k\,=\,1}^{k_0-1} |k\rangle\langle k|, \quad E_1 = \sum_{k\,=\,k_0}^{d} |k\rangle\langle k| \tag{B.8}$$

Therefore we have

$$P_e = \pi_0 - \sum_{k\,=\,1}^{k_0-1} |\lambda_k| = \pi_1 - \sum_{k\,=\,k_0}^{d} |\lambda_k|. \tag{B.9}$$

Add two terms together, we get

$$P_e = \frac{1}{2}\left(1 - \sum_k |\lambda_k|\right) = \frac{1}{2}\left(1 - \mathrm{Tr}|\Gamma|\right), \tag{B.10}$$

where $|\Gamma| = \left(\Gamma^{\dagger}\Gamma\right)^{\frac{1}{2}}$, i.e. the norm of Γ. The trace norm $\mathrm{Tr}|\mathrm{A}|$ ranges from 0 to 1, therefore error probability ranges from 0 (two states are orthogonal therefore perfectly distinguishable) to 0.5 (random guessing).

If there are N > 1 identical copies of the quantum state upon which meascurements can be performed. One could imagine making a sophisticated measurement on all N quantum systems at once. The Helstrom operator becomes

$$\Gamma_N = \pi_1 \rho_1^{\otimes N} - \pi_0 \rho_0^{\otimes N}, \tag{B.11}$$

which is hard to evaluate because of high dimensionality. One more drawback is that the Helstrom limit is not monotonicity under taking tensor powers. One can easily find states $\rho,\ \sigma,\ \rho',\ \sigma'$ such that $\mathrm{tr}|\rho - \sigma| < \mathrm{tr}|\rho' - \sigma'|$ but $\mathrm{tr}|\rho^{\otimes 2} - \sigma^{\otimes 2}| > \mathrm{tr}|\rho'^{\otimes 2} - \sigma'^{\otimes 2}|$.

For the trace distance and quantum fidelity for states ρ_0 and ρ_1, we have the following relation

$$\frac{1}{2}\mathrm{Tr}|\rho_0 - \rho_1| \leq \sqrt{1 - \left(\mathrm{Tr}\sqrt{\rho_0^{1/2}\rho_1\rho_0^{1/2}}\right)^2}. \tag{B.12}$$

When $\pi_0 = \pi_1 = 0.5$, we can derive that

$$P_e(N) \geq \frac{1}{2}\left(1 - \sqrt{1 - \mathrm{Tr}\left[\rho_0^{1/2}\rho_1^{1/2}\right]^{2N}}\right), \tag{B.13}$$

which gives a lower bound for the Helstrom limit.

B.3 Quantum chernoff bound

Given N identical copies of a state drawn from ρ_0 and ρ_1 with probability π_0 and π_1 respectively, the Helstrom limit is given by

$$P_e = \frac{1}{2}\left(1 - \mathrm{tr}|\pi_1\rho_1^{\otimes \mathrm{N}} - \pi_0\rho_0^{\otimes \mathrm{N}}|\right). \tag{B.14}$$

The quantum Chernoff bound [101] gives an asymptotically tight uppper bound for the Helstrom limit.

$$P_e(N) \leq \lambda_{\mathrm{QCB}}^N, \tag{B.15}$$

where

$$\lambda_{\mathrm{QCB}} = \min_{0\leq s\leq 1} \mathrm{Tr}|\rho_0^s \rho_1^{1-s}|. \tag{B.16}$$

It can be proved that $\mathrm{Tr}\left[A+B-|A-B|\right]/2 \leq \mathrm{Tr}|A^s B^{1-s}|$. Now let $A = \pi_0\rho_0^{\otimes N}$ and $B = \pi_1\rho_1^{\otimes N}$, we have

$$\begin{gathered}
\mathrm{Tr}[\pi_0\rho_0^{\otimes N} + \pi_1\rho_1^{\otimes N} - |A-B|]/2 \leq \mathrm{Tr}|\pi_0^s\pi_1^{1-s}\rho_0^{s\otimes N}\rho_1^{(1-s)\otimes N}| \\
[\pi_0(\mathrm{Tr}\rho_0)^N + \pi_1(\mathrm{Tr}\rho_1)^N - \mathrm{Tr}|A-B|]/2 \leq \pi_0^s\pi_1^{1-s}\mathrm{Tr}|\rho_0^s\rho_1^{1-s}|^N \\
\frac{1}{2}\left(1-\mathrm{Tr}|A-B|\right) \leq \min_{0\leq s\leq 1} \mathrm{Tr}|\rho_0^s\rho_1^{1-s}|^N
\end{gathered} \tag{B.17}$$

The last equation is exactly

$$P_e(N) \leq \lambda_{\mathrm{QCB}}^N \tag{B.18}$$

APPENDIX C

CODE SAMPLE FOR NUMERICAL CALCULATIONS

C.1 Code sample for creating density matrix in `laser2mode.py`

```
""" two-mode laser, TMSS and non-Gaussian states """

import qutip as qu
import numpy as np

class LaserTwoMode(object):
   """A class for two-mode lasers"""

   def __init__(self, l, n_max):
      """
      To initialize a two-mode state.
      Parameters
      ----------
      l: float
      lambda factor defined in equations of states
      n_max: integer
      maximum photon number for calculation is n_max - 1
      Return
      -----
      ValueError:
      when n_max is not valid
      """
```

```
        if n_max > 0:
            self.n_max = n_max
            self.lmd = l
            self.state_name = None
            self.state = None
        else:
            raise ValueError("N must be a positive integer.")

class TMSS(LaserTwoMode):
    """
    Two-mode squeezed state |TMSS \rangle = sum_0^n \lambda^n |n,
        n\rangle
    Parameters
    ----------
    l: double float
    state parameter, for TMSS l = tanh(s), where s is the squeezed para
    n_max: positive int
    photon truncation number as we are doing numerical calculation
    expr.set_input_laser(s_name, l) i.e. photon numbers can be in [0,
        n_max - 1]
    Return
    ------
    qutip.Qobj()
    a qutip object, a TMSS in bra form (column vector)
    """

    def __init__(self, l, n_max):
        super().__init__(l, n_max)
        self.state_name = "TMSS"
```

```
        self.state = qu.Qobj(np.sum([l ** n * qu.tensor(qu.basis(n_max,
            n), qu.basis(n_max, n))
        for n in np.arange(n_max)[::-1]])).unit()
        self.num = qu.expect(qu.num(self.n_max), self.state.ptrace(0)) *
            2
        self.exact_num = l ** 2 / (- l ** 2 + 1) * 2
        self.entanglement = qu.entropy_vn(self.state.ptrace(0))


class PS(LaserTwoMode):
    def __init__(self, l, n_max):
        """
        Photon subtracted state |PS> = a b |TMSS>
        Parameters
        ----------
        l: double float
        state parameter, for TMSS l = tanh(s), where s is the squeezed
            para
        n_max: positive int
        photon truncation number as we are doing numerical calculation
        i.e. photon numbers can be in [0, n_max - 1]
        Return
        ------
        qutip.Qobj()
        a qutip object, a photon subtracted state in bra form
        """
        super().__init__(l, n_max)
        self.state_name = "PS"
```

```
        self.state = qu.Qobj(np.sum([(n + 1) * l ** n *
            qu.tensor(qu.basis(n_max, n), qu.basis(n_max, n))
        for n in np.arange(n_max)[::-1]])).unit()
        self.num = qu.expect(qu.num(self.n_max), self.state.ptrace(0)) *
            2
        self.exact_num = 4 * l ** 2 * (l ** 2 + 2) / (1 - l ** 4)
        self.entanglement = qu.entropy_vn(self.state.ptrace(0))
```

C.2 Code sample for running simulations `qi.py`

```
""" Quantum Illumination """

import numpy as np
import qutip as qu
from scipy.sparse import spdiags
from scipy.optimize import minimize
from qutip.sparse import sp_eigs

from qillumi import laser2mode as l2m

class QIExpr(object):
    """
    Automatically numerical quantum illumination experiment
    """

    def __init__(self, n_max):
        """
        Initialize the QuIllumin object.
        Set the maximum photon number used for numerical simulation
        """
```

```
        self.n_max = n_max    # Fock numbers are in [0, n_max - 1]
        self.laser = None     # laser used for experiment
        self.reflectance = None # reflectance of the beam splitter
        self.nth = None       # average photon number of the thermal state
        self.thermal_0 = None # thermal state where an object may be
            embedded in
        self.thermal_1 = None # thermal state adjusted by the reflection
            factor
        self.qhb = None
        self.qcb = [0.5, 0.5]

    def __create_laser(self, name, l, rs=False):
        """
        Setup the entangled laser source for detection
        """
        laser = None

        if name == 'TMSS':
            laser = l2m.TMSS(l, self.n_max)
        elif name == 'PS':
            laser = l2m.PS(l, self.n_max)
        elif name == 'PA':
            laser = l2m.PA(l, self.n_max)
        elif name == 'PSA':
            laser = l2m.PSA(l, self.n_max)
        elif name == 'PAS':
            laser = l2m.PAS(l, self.n_max)
        elif name == "PCS":
            laser = l2m.PCS(l, self.n_max, rs)
```

```
        return laser

    def set_input_laser(self, state_name, lmd, rs=False):
        """
        Setup the two-mode entangled laser as input
        Parameters
        ----------
        state_name: string
        to specific what kind of laser as an input
        lmd: float
        lambda parameter for the laser, lmd = (N / (1 + N)) ** 0.5
        rs: 2-elements tuple of float
        used for PCS state
        Returns
        -------
        no return, alternate self.laser inplace
        """
        self.laser = self.__create_laser(state_name, lmd, rs)

    def set_environment(self, reflectance, nth):
        """
        Set up the thermal noise bath
        Parameters
        ----------
        reflectance: float
        reflectance of the possibly-exciting target object
        nth: float
        average photon number of the thermal noise
```

```
    Returns
    -------
    no return, alternate self.thermal_0 and self.thermal_1 inplace
    """
    self.reflectance = reflectance
    self.nth = nth
    self.thermal_0 = qu.thermal_dm(self.n_max, nth)
    self.thermal_1 = qu.thermal_dm(self.n_max, nth / (1 -
        self.reflectance))

def __evolve_rho0(self):
    """
    Output state rho 0 if an object is absent
    """
    rho_ab = qu.ket2dm(self.laser.state)
    return qu.tensor(rho_ab.ptrace(0), self.thermal_0) # rho_A
        (index 0) is kept here.

    def __evolve_rho1(self):
    """
    Output state rho 1 if an object is present
    """
    rho_ab = qu.ket2dm(self.laser.state)
    rho_abc = qu.tensor(rho_ab, self.thermal_1)

    xi = np.arcsin(np.sqrt(self.reflectance))

    # state A unchanged, tm_mixing acted on state B and thermal
    op = qu.tensor(qu.qeye(self.n_max), l2m.tm_mix(xi, self.n_max))
```

```
    rho_1 = op * rho_abc * op.dag()

    # Notice that we kept 0, and 1, as the order of a, b, c is kept
       after

    # mixing when we use the second labeling method
    return rho_1.ptrace([0, 2]) # keep A and B' (index 0, 2 for the
       second labeling method)


def qu_helstrom(rho0, rho1, p0=0.5, M=1):
    """ Calculate Helstrom error probability
    which is defined as
    P_e = 0.5 (1 - ||p1 * rho1 - p0 * rho0||)
    pi_0, rho_0: state 1 and its a priori probability pi_0
    pi_1, rho_1: state 2 and its a priori probability pi_1
    M: number of copies
    || rho || is the trace norm
    """
    if M == 1:
        q1 = 0.5 * (1 - ((1 - p0) * rho1 - p0 * rho0).norm())
        return q1
    else:
        pass # TODO: for those M != 1


def qcb_s(s, rho0, rho1):
    """
    Tr[rho ** s - rho ** (1 - s)]
```

```
    """
    return (power(rho0, s) * power(rho1, 1 - s)).tr().real


def qu_chernoff(rho0, rho1, approx=False):
    """ Approximated Q for QCB
    Actually the trace of sqrt(rho_1) * sqrt(rho_2)
    """
    if approx:
    # s = 0.5
        return 0.5, (rho0.sqrtm() * rho1.sqrtm()).tr().real
    else:
        res = minimize(qcb_s, np.array([0.5]), args=(rho0, rho1,),
            method='L-BFGS-B', bounds=[(0, 1)])
    s = res.x[0]
    if 0 <= s <= 1:
        return s, qcb_s(s, rho0, rho1)
    else:
        raise ValueError("s should be within [0, 1].")
```